Exposure to (micro/nano)-plastics and their combustion products studied by cyclic ion mobility-mass spectrometry

By

Mahin Hashemihedeshi

A thesis submitted to the School of Graduate Studies in partial fulfillment of the requirements for the degree of Master of Science (M.Sc.).

Department of Chemistry, Faculty of Science
Memorial University of Newfoundland

St. John's, Newfoundland and
Labrador, Canada

December 2023

Abstract

Degradation of plastics in the environment has led to formation of micro/nano-plastics (MNPs). Currently, there are only a few studies measuring plastic particles smaller than 1 μm in air. As such, the goal of this study was to develop a method for identification and quantification of MNPs in indoor air. Particulate matter (PM) from two indoor environments was size-resolved using a Micro-Orifice Uniform Deposit Impactor (MOUDI) model 110 cascade impactor ranging from 56 nm to 18 μm in size. The GCxcIM-MS method was then developed to characterize four common plastics: polystyrene (PS), polyethylene (PE), polypropylene (PP), and polymethyl methacrylate (PMMA). The results indicated that approximately 57-67% of MNPs had particle diameters >2.5 μm, and these microplastics constituted 50-60% of the total particulate matter in private residences. Moreover, the comprehensive two-dimensional separation provided by the developed method enabled us to analyze other polymers and plastic additives. For instance, plastic additives such as TDCPP (Tris (1, 3-dichloro-2-propyl) phosphate) was detected, and its concentration correlated with polyurethane (PU).

Plastic can also pose a risk to human health when they are combusted. The goal of second chapter was differentiation between toxic and non-toxic halogenated of polycyclic aromatic hydrocarbons (HPAHs) isomers that were released during combustion of plastics. The geometry of cIM-MS allows ions to travel multiple passes through cyclic cell such that, the greater of pass numbers, the better resolution of isomers. When a complex real sample was studied in this way, the toxic 2367-tetrachloroanthracene (2367-TCA) was separated from a mix of 17 other isomers with the assistance of an advanced "unwrapping" data analysis technique.

Acknowledgment

Co-authorship Statement

The author accomplished most of the experiments and data analysis of this thesis during two years of master's study in the field of analytical chemistry at the Memorial University of Newfoundland under the supervision of Dr. Karl Jobst. The main goal of this thesis was to develop a method for investigating the plastic pollutants in indoor air and study on their combustion products. The author is responsible for writing the initial draft for all the chapters of the thesis. Grammarly and ChatGPT 3.5 were employed to review the grammar and spelling in the initial drafts of Chapters 1, 2, 3, and 4. In addition, Chapters 1 and 3 were sent to the writing center of Memorial University of Newfoundland for their assistance regarding the grammar check.

Chapter 1 is based on reviewing the collected references and the author is responsible for reviewing and revising this chapter based on the comments. Chapter 2 is based on the following manuscript: "Size-resolved identification and quantification of micro/nano-plastics in indoor air using pyrolysis gas chromatography-ion mobility mass spectrometry" that has been submitted for reviewing in Journal of the American Society for Mass Spectrometry. The author designed the experiment, handled data acquisition and interpretation, created figures and tables and authored the manuscript. The first draft was reviewed and revised by Dr. Karl Jobst. The author expressed deepest gratitude to the collaborators and providers helped in this study. Ethan Haywood, who assisted during the sampling and sample preparation; Dr. Frank Dorman, who provided gas chromatography instrumental; Dr. Liisa Jantunen, who provided cascade impactor; and Daniel Gatch, who helped to install Pyrolyzer. The author expresses sincere appreciation to Dr. Lindsay Cahill, Dr. Paul Helm, and Dr. Miriam Diamond for their valuable discussions and support in interpreting the data. Chapter 3 is based on the following manuscript "Differentiating toxic and

List of publications

1. Breen, J.; Hashemihedeshi, M.; Amiri, R.; Dorman, F. L.; Jobst, K. J. Unwrapping Wrap-around in Gas (or Liquid) Chromatographic Cyclic Ion Mobility–Mass Spectrometry. Analytical Chemistry 2022, 94 (32), 11113-11117.

2. Amiri, R.; Bissram, M. J.; Hashemihedeshi, M.; Dorman, F. L.; Megson, D.; Jobst, K. J. Differentiating Toxic and Nontoxic Tricresyl Phosphate Isomers Using Ion–Molecule Reactions with Oxygen. Journal of the American Society for Mass Spectrometry 2023, 34 (4), 640-648.

3. Hashemihedeshi, M.; Haywood, E.; Gatch, D.; Jantunen, L.; Helm, P.; Diamond, M.; Dorman, F. L.; Cahill, L.; Jobst, K.J. Size-resolved identification and quantification of micro/nanoplastics in indoor air using pyrolysis gas chromatography-ion mobility mass spectrometry Journal of the American Society for Mass Spectrometry. (2023), pre-review.

Contents

List of Figures

List of Tables

List of Abbreviations

Abbreviation	Description
AC	Alternating current
AFM	Atomic force microscopy
AF$_4$-MALS	Asymmetric flow field-flow fractionation with multi aged light scattering
AF$_4$-TOC	Asymmetric flow field-flow fractionation with total organic carbon
AhR	Aryl hydrocarbon receptor
APCI	Atmosphere pressure chemical ionization
ASE	Accelerate solvent extractor
BFRs	Brominated flame retardants
CCS	Collision cross section
CI	Chemical ionization
CID	Collision induced dissociation
cIM	Cyclic ion mobility
EPS	Expanded polystyrene
DART	Direct analysis in real time
DBP	Dibutyl phthalate
DC	Direct current
DCM	Dichloromethane
DEHA	Di(2- ethylhexyl) adipate
DEHP	Di(2- ethylhexyl) phthalate
DEP	Diethyl phthalate
DIBP	Diisobutyl phthalate

DLC	Dioxin like compound
dl-PCB	Dioxin like polychlorinated biphenyls
DLS	Dynamic light scattering
DMF	Dimethylformamide
DOA	Dioctyl adipate
DPP	Dipentyl phthalate
DTIMS	Drift time ion mobility spectrometry
EI	Electron impact
EDX	Energy dispersive X-ray
FAIMS	Field asymmetric waveform ion mobility spectrometry
FRs	Flame retardants
FT-IR	Fourier transform infrared spectroscopy
GC	Gas chromatography
GF/F	Glass fiber filter
HBCDD	Hexabromocyclododecane
HRMS	High-resolution mass spectrometry
HPAH	Halogenated polycyclic aromatic hydrocarbon
KE	Kinetic energy
LC	Liquid chromatography
LCCP	Long chain chlorinated paraffins
LOD	Limit of detection
LOQ	Limit of quantification
MALDI	Matrix-assisted laser desorption ionization
MCCP	Medium chain chlorinated paraffins

MDL	Method detection limit
MNPs	Micro/nano-plastics
MPs	Microplastics
MOUDI	Micro-orifice uniform deposit impactor
NFPA	National fire protection association
NPs	Nanoplastics
NDT	Nanoparticle tracking analysis
OPAs	Organic plastic additives
OPFRs	Organo phosphate flame retardants
PBDE	Poly brominated diphenyl ethers
PAEs	Phthalic esters
PAHs	Polycyclic aromatic hydrocarbons
PCBs	Polychlorinated biphenyls
PCDD	Polychlorinated dibenzo-p-dioxin
PCDF	Polychlorinated dibenzo furan
PC	Polycarbonate
PE	Polyethylene
PET	Polyethylene terephthalate
PiFM	Photo induced forced microscopy
PLE	Pressurized liquid extraction
PM	Particulate matter
PMMA	Poly methyl methacrylate
POPs	Persistent organic pollutants
PP	Polypropylene

PS	Polystyrene
PUF	Polyurethane foam
PVC	Polyvinyl chloride
PXDD	Poly mixed bromo/chloro dibenzo-p-dioxin
PXDF	Poly mixed bromo/chloro dibenzo furan
Pyr-GC/MS	Pyrolysis-gas chromatography/mass spectrometry
R	Resolution
RF	Radio frequently
SBR	Styrene butadiene rubber
SCCP	Short chain chlorinated paraffins
SE	Solvent extraction
SEM	Scanning electron microscopy
SERS	Surface-enhanced Raman spectroscopy
SD	Standard deviation
SP-ICP-MS	Single particle-inductively coupled plasma-mass spectrometry
SVOC	Semi-volatile organic substance
TCEP	Tris(2-chloroethyl)phosphate
TCDD	Tetra chlorodibenzo-p-dioxin
TDCPP	Tris(1,3- dichloro-2-propyl)phosphate
TDI	Toluene diisocyanates
TEM	Transmission electron microscopy
TED-GC-MS	Thermal extraction desorption-gas chromatography-mass spectrometry
TEQ	Toxic equivalency quantity
ToF	Time of flight

TQ-FTICR	Tri quadrupole- Fourier transform ion cyclotron resonance
TWIMS	Traveling wane ion mobility spectrometry
UNEP	United Nation environment program
WHO	World Health Organization
XPS	X-ray photoelectron spectroscopy

List of Symbols

Symbol	Description
Å	Angstrom
t_a	arrival time
k_b	Boltzman constant
°C	degree centigrade
cm	centimeter
Ω	collision cross section
C	Coulomb
ρ	density
d	diameter
t_D	drift time
E	electric field
z	ion charge
h	hour
kg	kilogram
L	length
C_m	mass concentration
m_N	mass of neutral gas
m_I	mass of ion
μA	microampere
μm	micrometer

μs	microsecond
min	minutes
mm	millimeter
ms	milliseconds
N_2	molecular nitrogen
nm	nanometer
ppm	part per million
C_n	particle concentration
P	pressure
μ	reduced mass
s	second
T	temperature
V	voltage

Chapter 1. Introduction

1.1. Micro/nano-plastics definition

Plastics are an inseparable part of human life. Plastics are made of polymers. Polymers are categorized into two groups: natural polymers such as silk, wool, cellulose, and proteins; synthetic polymers such as nylon, Teflon, and polyester. Plastics are in the group of synthetic polymers that are made by petroleum oil [1, 2]. Utilizing plastic reduces product weight and due to their resistance and durability, they help to save resources [3]. However, the broad use of plastic products has raised concerns regarding their degradation. The degraded plastic particles are classified into two groups: microplastics (MPs) and nano-plastics (NPs) that are smaller than 5 mm and 1 µm, respectively [4].

The (micro/nano)-plastics (MNPs) are detected in soil and sediments [5], water [6], air [7], and food [8]. There are three routes of exposure to MNPs: ingestion, inhalation, and dermal contact [9]. Xu et al. reviewed research papers about potential impact of MNPs on mammalian systems [10]. The phrases and terms that they used in their research are: "human", "cell", "microplastics", "nano-plastics", "polystyrene", "effect", and "mice" [10]. They mentioned among 133 scientific articles covered in the review, 16 articles showed that MNPs did not have a significant impact on mammalian health. In contrast, 117 articles detected various health issues regarding exposure to MNPs like damage to genes, embryos, liver and the nervous system. The results have shown that submicron plastics (characterized by dimensions below 1 µm) have the potential to enter lung cells through inhalation [10]. Subsequently, these particles may translocate to secondary organs through

circulation within the bloodstream. Therefore, identification and quantification of MNPs in environmental areas is important [11].

1.2. MNPs in indoor and outdoor air

Daily, humans inhale approximately 9.3-16.2 m^3 of air [12], and during this process, various chemical compounds and particles can enter our bodies. People spend time in indoor and outdoor environments based on their age, occupation and circumstances. Geng et al. detected 43 ± 16 MPs particles per m^3 during inhaled indoor area and their results highlighted the importance of the study of indoor air [13]. In the study by Vianello et al. [14], they simulated human exposure to indoor airborne microplastics using a breathing thermal manikin. Their results showed the concentration of MPs was in the range of 1.7 to 16.2 particles/m^3. They showed that indoor environments have a substantial risk of microplastic exposure [14]. Smaller plastic particles have the capability to infiltrate deeply into the respiratory system, including the human lungs [9]. Also, the high surface area of NPs increases their ability to absorb organic pollutants and heavy metals. This property and their ability to transfer across different organisms underscores the need for more investigation on them [2]. However, due to technological limitations, accurately detecting the NPs is a significant challenge and the number of studies on atmospheric NPs are limited [2].

1.3. Plastic additives

Organic plastic additives (OPAs) have been used for enhancing polymer performance, malleability, functionality, and aging properties of plastic productions. OPAs have been divided into different groups like plasticizers, flame retardants, and light and heat stabilizers [15, 16].

1.3.1. Plasticizers

Plasticizers are utilized to enhance the flexibility, durability, and stretchiness of plastics while reducing their melt flow characteristics [16]. The common plasticizers that are used in the production of polyvinyl chloride (PVC) are phthalic esters (PAEs) like bis(2-ethylhexyl) phthalate (DEHP). The aforementioned plasticizers are approximately 80% of the whole plasticizer in PVC products. Plasticizers that frequently are used for PET products are dipentyl phthalate (DPP), di-(2-ethylhexyl) adipate (DEHA), di-octyl adipate (DOA), diethyl phthalates (DEP), diisobutyl phthalate (DIBP), and dibutyl phthalate (DBP) [16]. Numerous studies have reported health risks resulting from exposure to phthalates, including disturbances to the endocrine system and neurobehavioral disorders. These effects not only impact human health directly but also, they can increase the risk of diabetes, obesity, and cancer [17].

1.3.2. Flame retardants

Flame retardants (FRs) are used for reducing fire hazards over the years [18]. FRs encompass a range of substances, including short, medium, and long chain chlorinated paraffin (SCCP/MCCP/LCCP), brominated flame retardants (BFRs), and organophosphate flame retardants (OPFRs) [19].

BFRs were used in plastic products through chemical reactions or simple mixing. BFRs are bioaccumulative and toxic to humans and animals [19]. Polybrominated diphenyl ethers (PBDEs) are in the group of BFRs. In 2009, the United Nations Environment Program (UNEP) added Octa-BDE and Penta-BDE to the persistent organic pollutants (POPs) list [20]. OPFRs were introduced as an alternative for BFRs [20]. OPFRs are divided into three groups: organic, inorganic, and

halogenated compounds. The replacement for BFRs should not be environmentally persistent, bioaccumulative and toxic. Researchers have studied the health and environmental risks of identified halogenated OPFRs like tris(2-chloroethyl)phosphate (TCEP) and tris(1,3- dichloro-2-propyl)phosphate (TDCPP). Halogenated OPFRs increase flame retardant's lifetime by reducing mobility within the polymer matrix [21]. TDCPP is the common flame retardant that has been used in 36% of plastic products and polyurethane foams (PUFs) [22]. They have limited degradation in sewage sludge and natural waters [22]. The persistence of TDCPP highlights the need for detection and quantification of this pollutant. Another example of flame retardants is hexabromocyclododecane (HBCDD), which is commonly used as a flame retardant for polystyrene (PS) products. The study on oysters showed the level of HBCDD concentration increased in oysters that were near to PS [16]. These results underscore the study of plastic additives that are utilized in plastic production.

1.4. Plastic combustion products

Annually, the rate of plastic production increases around 5% [23]. Toys, packaging, containers, furniture, and medical devices are examples of plastic products. As a result, a large number of plastic wastes are generated. Most plastic waste is disposed of in landfills or incinerated. The incineration of plastic releases contaminants such as black smoke and volatile compounds [24, 25]. Burning of plastics in the presence of chlorine compounds produces chemical compounds like polychlorinated dibenzo-p-dioxins (PCDDs) and dibenzofurans (PCDFs). Research by Haibo et al. [26] has shown molecular oxygen (O_2) plays a role in the formation of these toxic compounds during combustion. O_2 can generate more active Cl_2 and promote chlorination. The result of their study showed the absence of oxygen significantly reduced the formation of the most harmful types

4

of PCDD/F compounds.

Plastic waste incineration produces air pollution such as carbon monoxide, particulate matter (PM), hydrochloric acid, and polycyclic aromatic hydrocarbons (PAHs) [27]. For those people who are directly exposed to plastic incineration, air pollution can be the cause of chronic diseases. For instance, half of firefighter fatalities are because of sudden cardiac events. Regarding these health risks, the National Fire Protection Association (NFPA) has published the standards and programs to improve firefighter well-being [28].

Accidental burning of plastics, like the Plastimet Inc. fire in Canada (1997) [29], released toxic compounds such as hydrogen chloride, PCDD, and PCDF into the environment. Advanced instruments helped researchers to identify the range of halogenated organic compounds. Fernando et al. [30] utilized GC × GC coupled with high-resolution time-of-flight mass spectrometry (ToF-HRMS) and triple quadrupole-Fourier transform ion cyclotron resonance (TQ-FTICR) for the study of samples from Plastimet Inc. Their study revealed that the combustion of PVC and other plastics released toxic compounds like PAHs and HPAHs besides halogenated dioxin/furan compounds. The concentration of compounds such as naphthalene, phenanthrene, fluoranthene, and pyrene, as well as their halogenated derivatives were determined. HPAHs were detected at levels of 20 µg/g in soil samples, while the concentration of dioxins/furans was around 40 ng/g. The results indicate the concentration of HPAHs were higher compared to dioxins and this fact highlights the importance of more research on HPAHs. In the study by Tu et al., they investigated the presence of Cl-PAHs and Br-PAHs in surface soil samples from an e-waste recycling site in Ghana [31]. Their findings revealed the Cl-PAH concentrations are in the range 160-220 (ng/g) and Br-PAHs range 19-46 (ng/g). Therefore, the toxicity of the uncharacterized halogenated PAHs

requires further investigation.

1.5. Air sampling method

Particulate matters (PMs) are a broad range of particles, including solid particles and liquid in the atmosphere [32]. PMs are known as pollutant in indoor and outdoor air. PMs are categorized into three groups based on their size: inhalable particles (PM_{10}) with a diameter of 10 micrometers or smaller, fine inhalable particles ($PM_{2.5}$) with a diameter of 2.5 micrometers or smaller, and ultrafine inhalable particles ($PM_{0.1}$) with a diameter of 100 nanometers or smaller [33]. Particles, especially $PM_{2.5}$, can pose serious health risks when inhaled and lead to respiratory and cardiovascular diseases. Although PMs are less than 1% of indoor and outdoor air, study of their impact on human health is necessary [34, 35]. PMs contribute to environmental pollution, affecting air, soil, and water quality. Overall, research on PM plays a pivotal role in shaping policies for air quality management, protecting ecosystems, and ensuring the well-being of communities.

Air sampling is a process to collect airborne contaminants for controlling the air quality of indoor and outdoor air. There are two types of air samplers: passive air samplers (PAS) and active air samplers (AAS) [36]. AAS requires a pumping device to pass air through the sampler, whereas PAS method does not involve a pump. Although for utilizing AAS methods stable electricity and high maintenance are required, experiments with AAS are more reproducible than PAS. Since PAS have lower air sampling rates than AAS, they are often used in long sampling durations, such as those required for seasonal studies. For example, they have been used to study seasonal pollutants in the atmosphere [36]. Both methods can collect MNPs from the air, but since light particles do not tend to settle down by themselves, AAS can collect the smaller particles, such as $PM_{2.5}$ and

PM$_{0.1}$ [37].

Cascade impactor (shown in Figure 1.1) is a tool that can be used to collect PM from the air. The first cascade impactor was invented in 1945 for measuring the aerodynamic size distribution of aerosols [38]. This device is designed to separate and collect small particles according to their size [39]. As the aerosols pass through these stages, firstly they will be accelerated through the stage orifice. Then, the smaller particles change direction to follow the air streamline, but the larger particles are unable to turn, and they will collect on the impaction plate. The impaction plates are perpendicular to the flow direction and close to the exit of each orifice. Due to their ability to collect PM samples, they are a suitable device for collecting various sizes of MNPs from the air.
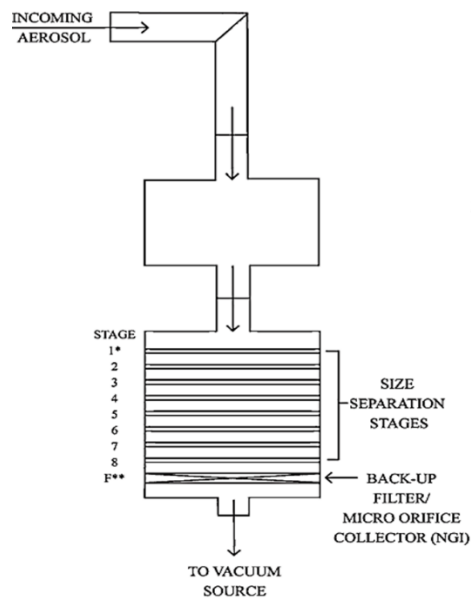
Figure 1.1. Schematic of cascade impactor. (Stage 1* provided the upper limit of measurement range. The backup stage** collects particles that have passed the previous stage). Figure adapted with authorization from Ref. [39].

1.6. Sample preparation

There are two methods for introducing plastic to instruments for identification and quantification of them and their additives: direct and indirect methods. Regarding the direct method, thermal methods should be highlighted (further details are provided in Section 1.7.3). Thermal methods would be used for direct separation of the additive from the polymeric matrix [40]. However, due to small sample sizes, thermal analysis faces challenges in quantification. Moreover, chemical compounds that are formed at high temperatures in complex environmental samples make a challenge for data analysis [41]. Due to challenges regarding the complexity of polymeric matrix, developing sensitive analytical methods is required. In indirect methods, such as solvent extraction (SE), the analysis is based on dissolving the samples and separating plastic and their additives from the sample matrix [15]. In the analysis of low-concentration analytes in environmental samples with complex matrix, it is crucial to precisely define the limit of detection (LOD) and limit of quantification (LOQ). SE analysis offers lower LOD and LOQ values compared to direct methods due to a pre-concentration step.

Accelerated solvent extractor (ASE) is a sample preparation method that was employed in this study. ASE is also known as pressurized liquid extraction (PLE). ASE, introduced in 1995 [42], offers advantages over traditional techniques like sonication and Soxhlet extraction [43]. Traditional methods have excessive solvent usage and time-consuming processes. ASE is known for its swift extraction capabilities and high pressure and temperature to enhance extraction efficiency. ASE is used to extract organic compounds from solid and semisolid matrices. Higher temperatures increase analyte solubility and diffusion of analytes by weakening interactions like Van der Waals forces, hydrogen bonding, or dipole interactions between the analytes and sorbent.

8

For example, the solubility of anthracene in an ideal solvent increases by a factor of 13 within the temperature range of 50 to 150°C [44]. Also, for water, solubility in nonpolar solvents increases at higher temperatures. As hydrogen bonding weakens with increased temperature, this aids the extraction of analytes that are initially in pores filled with water. Also, higher temperature reduces the solvent viscosity and surface tension of the solvent. These effects lead to better diffusion of solvent in the matrix [44].

ASE employs temperatures above the solvent's boiling point, so high pressure is necessary to keep the solvent in a liquid phase. The higher pressure also helps to push the solvent into the sample's pores. Additionally, a study by Lou et al. [45] showed a direct correlation between high pressure and higher recovery, especially during the extraction of polymer samples. ASE also provides a wide range of solvents for extracting different types of analytes even with solvents that were previously inefficient [46]. The schematic of ASE is shown in Figure 1.2.
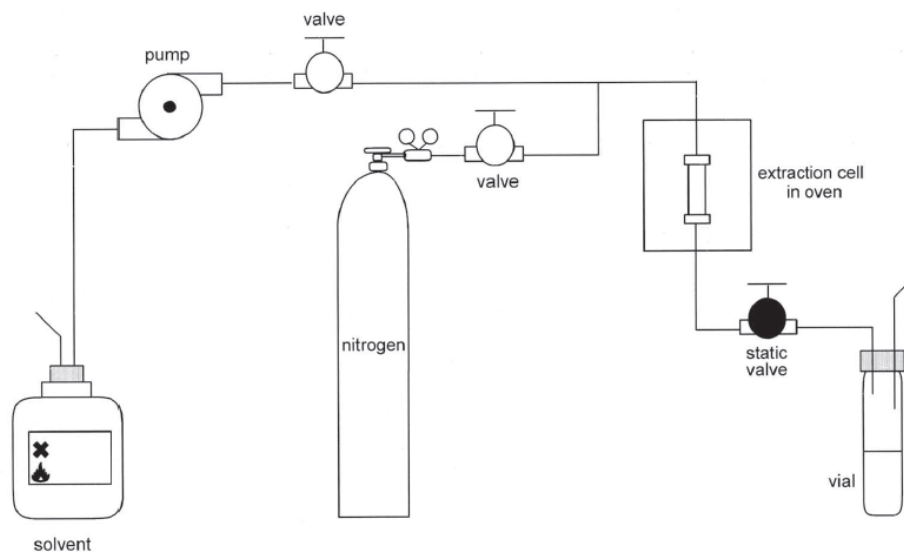
Figure 1.2. Schematic of accelerated solvent extraction setup. Figure adapted with authorization from Ref. [46].

The first step of ASE extraction is the weighing of the sample, which could be soil, tissues, or filters. Then, samples will be placed into the cell that are available in different sizes, from 10 to 100 mL. The cell is then placed into a preheated oven (see in Figure 1.2,) and the solvent flows into the loaded cell. The extraction procedure can occur in two modes: dynamic and static. In the static phase, the cell is heated along with the sample during an equilibration time. Multiple cycles during a single extraction leads to improving extraction recovery. After extraction, the sample is rinsed with fresh solvent, and the entire system is purged with nitrogen to remove the remaining solvent [46].

ASE is an appropriate method for extracting analytes from various samples with complex matrices. For instance, in a study by Alexandrou et al. [47], they utilized ASE to extract pollutants such as PAHs from atmospheric particulate matter collected on glass fiber filters [47]. Furthermore, ASE is an effective tool for extraction of microplastics from animal tissues and soil samples [48, 49]. Ribeiro et al. [50, 51] utilized ASE to extract different types of plastics such as PS, PE, PVC, PP, and PMMA from seafood samples.

1.7. Methods for identification and quantification of MNPs

There are several analytical methods for investigation on various MNPs properties, such as plastic dimensions, morphology [52], chemical fingerprints [53], and mass quantifications [49, 50, 54]. Microscopy, spectroscopy, and thermal methods are three common techniques for detection and quantification of MNPs.

1.7.1. Microscopy techniques

Microscopy techniques offer information about shape, structure, and surface characteristics of plastic particles [55]. Detection methods range from visual observation for larger particles to various microscopy types for smaller ones. For example, larger plastic particles (0.41 to 420 mm) have been detected visually [56]. For the study of smaller plastic particles, microscopic methods such as light microscopy, electron microscopy, and atomic force microscopy (AFM) can be utilized. Electron microscopy such as scanning electron microscope (SEM) and transmission electron microscope (TEM) uses electrons accelerated toward samples for imaging signals.

AFM reveals the morphology of plastic particles through using probes that interact with samples [57]. AFM as a non-destructive method offers benefits such as the ability to analyze samples with complex matrices [57]. Although microscopic methods provide information about plastic particles morphologies, they have some limitations such as human error, confusion between plastic particle and with natural materials, variations in sample thickness, light scattering due to plastic degradation, and the difficulty of detecting particles under 500 μm [58].

1.7.2. Spectroscopy techniques

Spectroscopic methods are used for identifying plastic particles. These methods can be combined with microscopes to enhance the accuracy of microplastic characterization. Spectroscopic techniques include Raman spectroscopy and Fourier transform infrared spectroscopy (FT-IR). FT-IR is a vibrational spectroscopy technique that utilizes infrared electromagnetic radiation (wavelength 400-4000 cm^{-1}). It is expected to compare obtained spectra with reference libraries to validate composition; with confidence intervals >70% [59]. One of the

limitations of FTIR is the size of particles and they should be larger than 10 μm [60]. However, Micro-FTIR [61] was introduced for smaller plastic particles; this technique can be significantly affected by the presence of organic matter on the surface of the plastic particles [60]. Raman spectroscopy, another vibrational spectroscopy method, employs a monochromatic laser instead of infrared radiation. FTIR and Raman provide spectra with specific chemical composition information, and they can complement each other [62].

1.7.3. Thermal techniques

Thermal techniques are introduced as a destructive method. Thermal techniques are important in scientific research due to their ability to extract unique information from materials. These techniques involve exposing a sample to extreme temperatures and subsequently studying the sample's decomposition products [63]. Thermal analysis can be combined with mass spectrometry (MS) to identify and quantify polymers [64].

Pyrolysis-gas chromatography/mass spectrometry (Pyr-GC/MS) is one of the common examples of combining thermal methods with mass spectrometry techniques. The Pyr-GC/MS process involves heating a sample to break down polymers. The pyrolyzed products can be separated using a GC and analyzed with MS [65]. Pyr-GC/MS is an appropriate tool in identifying the content of polymeric particles [66]. Pyr-GC/MS has been utilized in various studies focused on detecting MNPs in samples with complex matrices. Ter Halle and their colleagues detected NPs in colloidal debris in the North Atlantic subtropical gyre by Pyr-GC/MS [67]. Most of the detected NPs were PVC, polystyrene (PS), polyethylene (PE), and Polyethylene Terephthalate (PET). Also, their research confirmed the origin of aromatic hydrocarbons found in the samples and provided

insights into the chemical composition.

Combination of Pyr-GC/MS with ASE (explained in Section 1.6) makes it sufficient to analyze plastic particles in samples with complex matrices such as soil [54], rice [68], and fish tissue [50]. Advanced mass analyzers, such as ToF or orbitrap, can enhance plastic detection even at a smaller scale [69]. Pyr-GC-ToF is a sensitive method for quantifying plastics and the results of the study by this instrument showed the LOD of PVC and PS is less than 50 (μg/L) in water samples.

Thermal extraction desorption (TED) is another example of a thermal method that can be combined with GC/MS. TED-GC/MS operates like Pyr-GC/MS, relying on thermogravimetric analysis to decompose samples. In TED, the decomposition products and solid-phase absorbers are in the same region [70]. Therefore, TED has this capacity to analysis larger volumes of sample than Pyr-GC/MS. Dümichen et al. [63] demonstrated its suitability for detecting various plastics, such as PS, PP, and PE, in plant fermentation biogas without need for sample preparation.

The MS as an analytical tool can have different ionization chambers and mass analyzers depending on their application [71]. Matrix-assisted laser desorption ionization-time of flight mass spectrometry (MALDI-ToF-MS) is a method with soft ionization that can be used for detection and quantitation of plastic particles [72]. Zhang et al. [53] conducted a study using direct analysis in real time (DART)-HRMS to quickly identify and characterize microplastics. They created a "chemical fingerprint" of microplastics that they thermally decomposed. They analyzed the data using multivariate statistics method and elemental composition analysis. This method has the potential to identify the composition and sources of microplastics in the environment. In their study, they investigated various plastics from personal care products and aquatic environments and

separated plastic types based on their sources. Their results showed that this analytical approach is efficient for differentiating microplastic pollution based on their origins.

1.8. Instrumental analysis

In this thesis, gas chromatography (atmospheric pressure chemical ionization) cyclic ion mobility mass spectrometry (GC-(APCI)-cIM-MS) method was utilized. In addition, due to the advantages of thermal method combined with MS for identification and quantification of plastic particles, pyrolyzer was used for introducing MNPs into the instrument.

1.8.1. Pyrolysis–Gas Chromatography

Pyr-GC was employed for the analysis of plastics. In Pyr-GC, controlled heating is applied to break macromolecules into more volatile molecules. Then inert gas transports the pyrolyzed products to a GC column for separation. The temperatures of the GC column can reach up to 300°C to separate compounds in their gaseous form. The compounds will be separated based on their different affinity to the stationary phase of the GC column. Various pyrolyzers can be employed in Pyr-GC, such as Curie point, microfurnace, and filament [73].

Curie point pyrolyzer, utilizes inductively heated wire until the metal loses its ferromagnetic properties. Curie point pyrolyzer is limited to specific composition of metal for specific temperature. In the microfurnace pyrolyzer, samples are directly introduced into a high-temperature furnace chamber. Although the temperature of microfurnace is reproducible, due to hot regions in the furnace, secondary pyrolysis will happen, and their application is limited to lower temperatures. The other method for pyrolysis of samples is utilizing filaments that are wires or

strips of platinum. The advantage of this method is the temperature range is wide, from room temperature to 1000°C with 1°C precision. Moreover, this method is suitable for both liquid and solid samples. Samples are placed in a quartz tube, which is inserted into a coil-type filament (shown in Figure 1.3). The heating process in these pyrolyzers is designed to rapidly reach high temperatures, typically in less than a second, which is crucial for enhancing analyte separation by reducing peak widths [73].
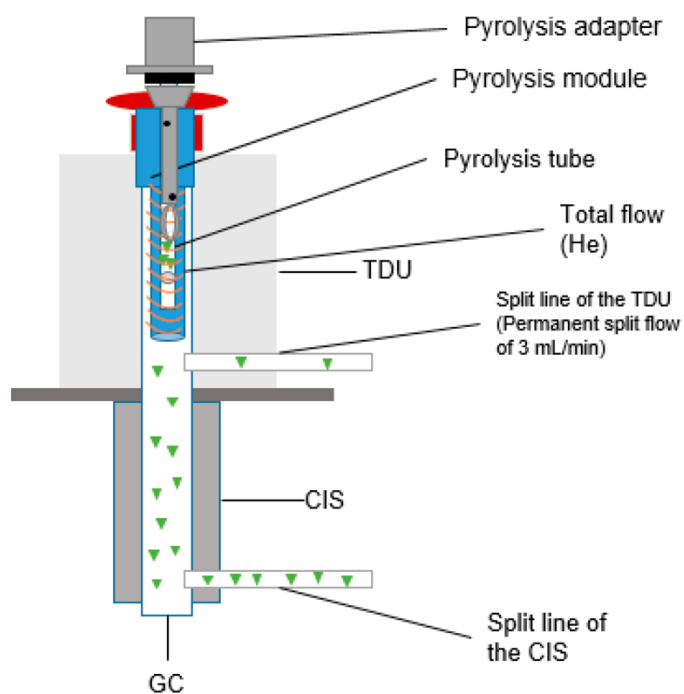
Figure 1.3. Schematic of filament for pyrolysis. Figure adapted with authorization from Ref. [74].

1.8.2. Ionization Techniques

Following the separation of compounds through GC, based on their physical properties,

such as their polarity and boiling point, they are transferred to an ionization chamber where they transform into ions. The ionization techniques ionize molecules based on their polarity, volatility, and stability and they are categorized in two groups: hard and soft ionization [75]. Electron impact (EI) is a hard ionization method, which is employed for compounds stabile at high temperatures with low molecular weights. In the EI chamber, there is a filament with 70 eV high-energy electrons that create a beam of electrons. The interaction between the beam of electrons and the sample molecules in the gas phase creates singly positively charged ions and resulting data can be compared with data from a mass spectrometry library [75, 76].

In this study, atmospheric pressure chemical ionization (APCI) was utilized, as a soft ionization method that reduces fragmentation compared to EI. In APCI, ionization occurs at atmospheric pressure [77]. For APCI function, makeup gas and compounds from the GC column enter the ionization chamber. The corona discharge needle ionizes the makeup gas. When nitrogen gas (N_2) is employed as the makeup gas in positive mode, it generates $N_2^{\bullet+}$ and $N_4^{\bullet+}$ ions, a plasma of primary ions. In high-pressure nitrogen plasmas, $N_4^{\bullet+}$ is formed in ion sources during discharging of N_2. N_2 has an ionization energy (IE) of 15.6 ± 1.2 eV, while N_4 has an IE of 10.3 ± 0.5 eV and in comparison, ionization energies of most organic compounds are in the range of 8-12 eV [78].

In an APCI ionization chamber, the charge transfer occurs between compounds and $N_2^{\bullet+}$ or $N_4^{\bullet+}$ [79]. During this process, the makeup gas (N_2) has higher concentrations compared to the sample and this leads to enhance the chance of chemical ionization rather than EI ionization [80]. The ionization reactions depend on the nature of the sample molecule and the reagent gas. These reactions can include proton transfer, proton abstraction, and the formation of adducts [81]. The

analyte becomes protonated or deprotonated depending on its proton affinity and gas-phase acidity [41]. Analyte (M) as proton acceptor must have a higher proton affinity than the proton donor ($H_3O^{\bullet+}$). The process of protonated analyte can be represented as follows:

$$H_2O + N_2^{\bullet+} \rightarrow H_2O^{\bullet+} + N_2$$

$$H_2O + H_2O^{\bullet+} \rightarrow H_3O^{\bullet+} + OH^{\bullet}$$

$$M + H_3O^{\bullet+} \rightarrow [M+H]^{\bullet+} + H_2O$$
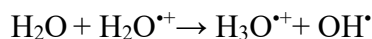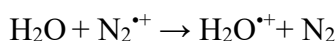
1.8.3. Tandem mass spectrometry

Following the ionization of compounds, the mixture of precursor ions will separate according to their mass-to-charge ratio (m/z). Tandem mass spectrometry is a technique that selects and then breaks down precursor ions into product ions for detecting the chemical structure of precursor ions [82]. In this research, the selected precursor ions initially undergo separation in the quadrupole mass analyzer. Subsequently, they are directed to the cyclic ion mobility for further separation before entering the second mass analyzer, which is tom of flight (TOF) Tandem mass spectrometry can be used to investigate polymer structure. The ions pattern can provide information about monomer sequences and their backbone [83, 84].

The quadrupole analyzer is designed with four parallel cylindrical rods. One set of opposite rods is connected to a positive direct current (DC) voltage, and the other pair is connected to the negative terminal. Additionally, alternating current (AC) voltage is applied to each pair of rods. Ions were accelerated, before entering quadrupole region. When only AC voltage is applied to two rods in positive cycle, positive ions tend to converge toward the center, while during the negative half, they tend to diverge. Positive ions based on their m/z and AC frequency strike the rods during

the negative AC phase and they become neutral and are removed. However, lighter ions collide with the rods during the negative AC, heavier ions do not tend to respond to the AC voltage and are influenced more by DC voltage [75, 85]. This capability allows the quadrupole to selectively filter compounds based on their m/z ratio [85]. The selected ions exiting the quadrupole region then enter the trap region for further collision-induced dissociation (CID) [82]. Optimized voltage can fragment the selected ions. This fragmentation can assist scientists in further characterization and identification of molecular structures [86].

ToF measures the time it takes for ions to travel between the entry point and the detector. The velocity is determined based on the distance between the entry point and the detector. In ToF instruments, ions are under an electric field pulse of 10^3 to 10^4 V to accelerate them. The time for each ion to reach the detector in a field-free drift tube is measured. Therefore, ions with the same kinetic energy will be separated based on their velocity (v) (Equation 1.1) [75].

$$v = \sqrt{\frac{2KE}{m}} \quad (1.1)$$

Equation 1. 1 showed variables: "m" represents the mass of ions (kg), and "KE" kinetic energy of particles (J). Based on this equation, lighter ions reach the detector faster than heavier ones. This mass analyzer offers advantages such as simplicity, high mass accuracy, fast scan speed, and the ability to analyze ions with a wide mass range. With this mass analyzer, the entire spectrum with more data is available. In this study, the instrument with a 40-centimeter ToF length and two operation modes: V mode and W mode was utilized. In W mode, triple deflection and an extended ToF chamber improve result resolution and ion separation compared to V mode [87].

1.8.4. Ion mobility spectrometry

Ion mobility spectrometry (IMS) is a combination of gas-phase ion mobility and mass spectrometry. Combination of IMS with liquid chromatography (LC) and gas chromatography (GC) introduces an additional dimension of separation [88]. The IMS principle is based on the measurement of the duration time for ions under electric field to traverse in a drift cell in the presence of a buffer gas such as helium (He) or nitrogen (N_2). This duration, known as drift time, varies for each ion due to the influence of an electric field and colliding with the buffer gas. Therefore, their mobility relies on factors such as ion size, charge, and shape [89]. The ions mobility has an inverse relationship to the ions collision cross section (CCS) [90]. CCS is calculated based on the average area of the ion interacting with a carrier gas [89]. The ions with larger CCS are under more collision by buffer gas than those with smaller CCS and have a longer drift time.

Various types of IMS technologies are available, including drift time ion mobility spectrometry (DTIMS), field asymmetric waveform ion mobility spectrometry (FAIMS), and traveling wave ion mobility spectrometry (TWIMS) [91]. The resolution (R) of each ion mobility technique is calculated based on Equation 1.2 [87].

$$R \sim \sqrt{\frac{LzE}{T}} \quad (1.2)$$

In this equation, the symbol "L" represents the length of the traveling cell, "E" stands for the electric field, "z" denotes the charge of the ion, and "T" represents the temperature of the buffer gas. According to this equation, the resolution power is directly correlated to the square root of the

length of the ion mobility (IM) cell. Increasing the path length, electric field, and decreasing temperature led to an increase in resolution. However, improving resolution is not possible by enlarging the cell size. Merenbloom et al. [92] developed multi-pass cyclotron ion mobility spectrometry. In this design, ions that resonate with the field switching frequency are isolated in the cyclotron device using sequentially applied electric fields. This process leads to an improvement in resolution.

1.8.5. Cyclic ion mobility

This study utilized cyclic TWIM. In standard TWIM a series of pulsed energy voltages is applied to the ions as they traverse the buffer gas. Pulsed energy voltage is achieved by utilizing a combination of radio frequency (RF) and direct current (DC) voltage applied along its length [87]. TWIM is an appropriate tool for multi-pass experiment, since the potential at the start and end of the TWIM is the same. By allowing ions to circulate multiple times within the cyclic device, they experience longer transit times and greater distances and this results in enhancing the ion mobility resolution power [93]. To achieve this higher resolution, one requires a new IMS instrument known as cyclic ion mobility (cIM) [94]. The important aspect of cIM is its capacity to carry out IMS^n experiments (n is pass number).

The cIM-MS employed in this study (Shown in Figure 1.4 A) [87] is in tandem with a quadrupole and ToF mass analyzer. In this new instrument, the cIM-MS is replaced by a standard TWIM device and is located orthogonally to the main ion axis (Figure 1.4 B). The packet of ions from the trap will be released into the cIM-MS for separation. Finally, the ions that have undergone mobility separation are expelled to the ToF mass analyzer for detection and recording their arrival

time.
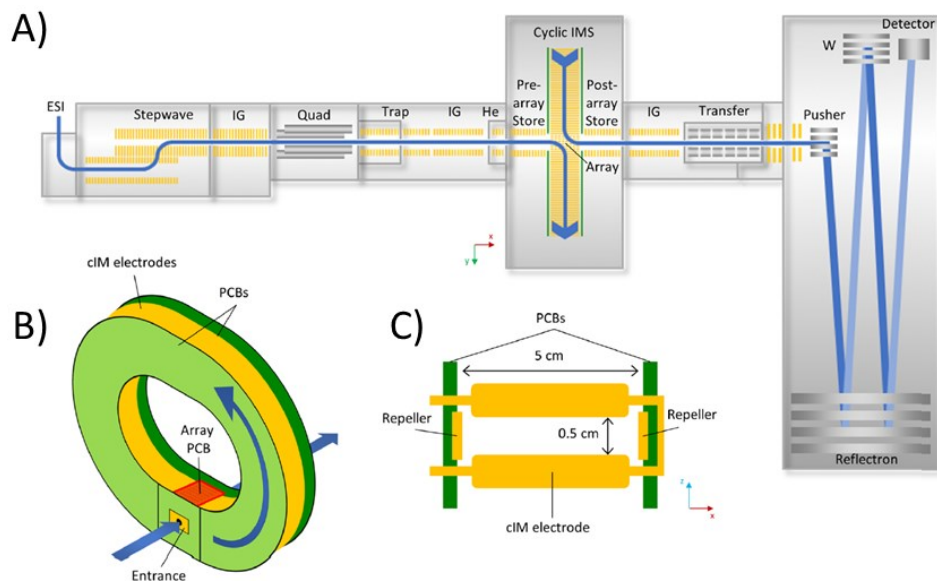
Figure 1.4. Schematic of quad-cIM-MS-ToF: (A) instrument overview; (B) cIM-MS; (D) cIM electrodes. Figure adapted with authorization from Ref. [87].

The cIM-MS device is designed for introducing ions, separating them based on their mobility and transferring them without compromising the resolution. The cIM cell has two main parts: ion entry/exit region and separator (Figure 1.4 B). The entry/exit region is before and after separator. There are two stacked ring ion guide (SRIG) systems in the pre-cIM chamber (shown as IG in Figure 1.4 A). The initial SRIG receives ions from the quadrupole, whether they have undergone resolution or not, gathers them and subsequently releases them as an organized packet of ions in the separator. The main body (separator) included 608 electrodes, and in the main separation region. The electrode structure forms a 0.5 cm × 5 cm rectangular ion transmission channel (Figure 1.4 C). The rectangular geometry of cIM-MS offers several advantages for a

21

closed-loop separator such as: enhanced charge capacity, reduced high voltage requirements, and minimized "Racetrack" effects [87].

The cIM-MS can differentiate isomers in multi-pass experiments due to its higher resolutions. In a study by Umja et al. [95], they utilized cIM-MS for separation of α and β penta saccharides through five passes. However, the high resolution achieved through multi-pass experiments faces limitations in complex sample matrices. In such cases, lighter ions with higher speed may surpass heavier ions with slower mobility, referred to as "wrap-around." In the study by Breen et al. [94], they addressed the wrap-around and proposed a method to "unwrap" data. They mentioned that for unwrapping multi-pass experiments, at least two experiments with zero passes (t_{0p}), setting separation time of 0.01 ms, and one single pass experiment, setting separation time of 1-2 ms were employed. These are the intercept and slope in Equation 1.3.

$$t_a = nt_{1p} + t_{0p} \quad (1.3)$$

In Equation 1.3 the pass number "n" of ions that travel around the cyclic cell can be measured by their arrival time "t_a". To extract the necessary data for unwrapping, they exported data from DriftScope software using pick peaking. The exported data from DriftScope includes ions' chromatographic retention time, arrival time, and m/z values. The calculated average period for each ion can be plotted versus m/z or retention time to generate an unwrapped plot. The plot of wrapped retention time versus periodic drift time (Figure 1.5 A) can also be unwrapped,

resulting in Figure 1.5 b. This method is beneficial for unwrapping isomers, as extensively detailed in the Chapter 3.
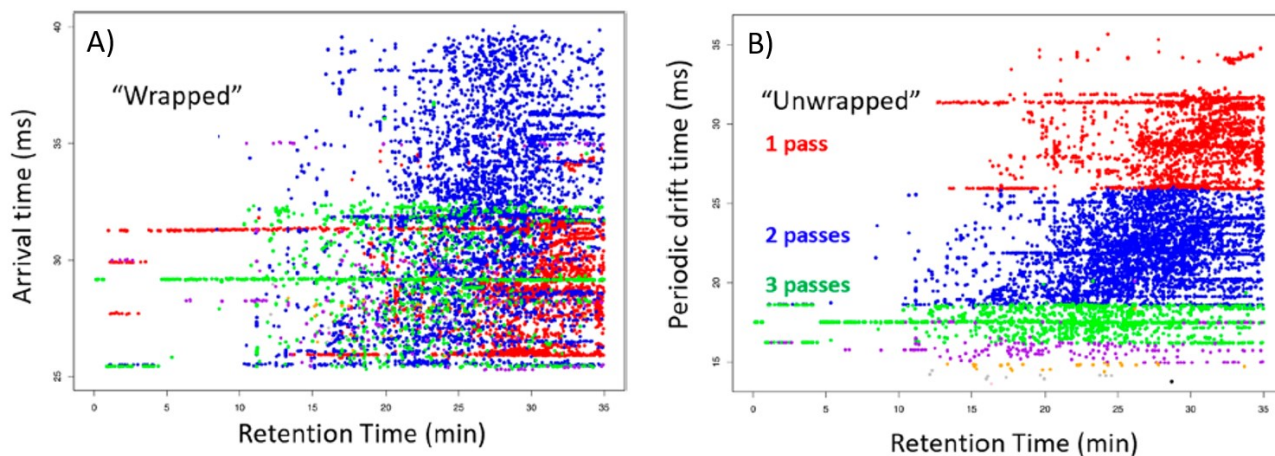
Figure 1.5. Retention time vs drift time contour plots of (A) "wrapped" and (B) "unwrapped". Figure adapted with authorization from Ref [94].

1.9. Objectives and Outlines

The primary purpose of this study is to develop a method for collecting, detecting, and quantifying MNPs in indoor air. The second chapter focuses on developing a method for identification and quantification of size resolved MNPs in indoor air. Also, the correlation between plastic concentrations and their plastic additives was investigated. The third chapter presents the results of experiments at distinguishing between toxic HPAHs isomers using multi-pass cIM techniques. To achieve these purposes, cIM-MS has been employed as a powerful tool for better understanding about toxic environmental contaminants. Lastly, the fourth chapter serves as a comprehensive summary of the thesis findings.

1.10. References

[1] Bhatia, S. Natural Polymers vs Synthetic Polymer. Springer International Publishing AG, 2016; pp 95-118.

[2] Bhat, M. A.; Gedik, K.; Gaga, E. O. Atmospheric micro (nano) plastics: future growing concerns for human health. *Air Quality, Atmosphere & Health* **2023**, *16* (2), 233-262.

[3] Andrady, A. L.; Neal, M. A. Applications and societal benefits of plastics. *Philosophical Transactions of The Royal Society B Biological Sciences* **2009**, *364* (1526), 1977-1984.

[4] Jiang, B.; Kauffman, A. E.; Li, L.; McFee, W.; Cai, B.; Weinstein, J.; Lead, J. R.; Chatterjee, S.; Scott, G. I.; Xiao, S. Health impacts of environmental contamination of micro- and nanoplastics: a review. *Environmental Health and Preventive Medicine* **2020**, *25* (1), 29.

[5] Hurley, R. R.; Nizzetto, L. Fate and occurrence of micro(nano)plastics in soils: Knowledge gaps and possible risks. *Current Opinion in Environmental Science & Health* **2018**, *1*, 6-11.

[6] Alimi, O. S.; Farner Budarz, J.; Hernandez, L. M.; Tufenkji, Microplastics and nanoplastics in aquatic environments: aggregation, deposition, and enhanced contaminant transport. *Environmental Science and Technology* **2018**, *52* (4), 1704-1724.

[7] Sridharan, S.; Kumar, M.; Singh, L.; Bolan, N. S.; Saha, M. Microplastics as an emerging source of particulate air pollution: A critical review. *Journal of Hazardous Materials* **2021**, *418*, 126245.

[8] Rainieri, S.; Barranco, A. Microplastics, a food safety issue? *Trends in Food Science & Technology* **2019**, *84*, 55-57.

[9] Abbasi, S. Routes of human exposure to micro(nano)plastics. *Current Opinion in Toxicology* **2021**, *27*, 41-46.

[10] Xu, J.-L.; Lin, X.; Wang, J. J.; Gowen, A. A. A review of potential human health impacts of micro- and nanoplastics exposure. *Science of the Total Environment* **2022**, *851*, 158111.

[11] Rodrigues, A. C. B.; de Jesus, G. P.; Waked, D.; Gomes, G. L.; Silva, T. M.; Yariwake, V. Y.; da Silva, M. P.; Magaldi, A. J.; Veras, M. M. Scientific Evidence about the Risks of Micro and Nanoplastics (MNPLs) to Human Health and Their Exposure Routes through the Environment. *Toxics* **2022**, *10* (6), 308.

[12] Allan, M.; Richardson, G. M. Probability Density Functions Describing 24-Hour Inhalation Rates For Use in Human Health Risk Assessments. *Human and Ecological Risk Assessment: An International Journal* **1998**, *4* (2), 379-408.

[13] Geng, Y.; Zhang, Z.; Zhou, W.; Shao, X.; Li, Z.; Zhou, Y. Individual Exposure to Microplastics through the Inhalation Route: Comparison of Microplastics in Inhaled Indoor Aerosol and Exhaled Breath Air. *Environmental Science & Technology Letters* **2023**, *10* (6), 464-470.

[14] Vianello, A.; Jensen, R. L.; Liu, L.; Vollertsen, J. Simulating human exposure to indoor airborne microplastics using a Breathing Thermal Manikin. *Scientific Reports* **2019**, *9* (1), 8670.

[15] Akoueson, F.; Chbib, C.; Monchy, S.; Paul-Pont, I.; Doyen, P.; Dehaut, A.; Duflos, G. Identification and quantification of plastic additives using pyrolysis-GC/MS: A review. *Science of the Total Environment* **2021**, *773*, 145073.

[16] Hahladakis, J. N.; Velis, C. A.; Weber, R.; Iacovidou, E.; Purnell, P. An overview of chemical additives present in plastics: Migration, release, fate and environmental impact during their use, disposal and recycling. *Journal of Hazardous Materials* **2018**, *344*, 179-199.

[17] Cohen, J. F. W.; Richardson, S.; March, W. W.; Gosliner, W.; Hauser, R. Phthalates, adipates, BPA, and pesticides in school meals. *Environmental Research* **2023**, *236*, 116632.

[18] Hansen, E.; Nilsson, N. H.; Lithner, D.; Lassen, C. Hazardous substances in plastic materials. *Science of the Total Environment* **2013**, 7-8.

[19] Kim, Y.-J.; Osako, M.; Sakai, S.-i. Leaching characteristics of polybrominated diphenyl ethers (PBDEs) from flame-retardant plastics. *Chemosphere* **2006**, *65* (3), 506-513.

[20] van der Veen, I.; de Boer, J. Phosphorus flame retardants: Properties, production, environmental occurrence, toxicity and analysis. *Chemosphere* **2012**, *88* (10), 1119-1153.

[21] Van der Veen, I.; de Boer, J. Phosphorus flame retardants: properties, production, environmental occurrence, toxicity and analysis. *Chemosphere* **2012**, *88* (10), 1119-1153.

[22] Stapleton, H. M.; Klosterhaus, S.; Keller, A.; Ferguson, P. L.; Van Bergen, S.; Cooper, E.; Webster, T. F.; Blum, A. Identification of flame retardants in polyurethane foam collected from baby products. *Environmental Science and Technology* **2011**, *45* (12), 5323-5331.

[23] Braun, D. J.Poly (vinyl chloride) on the way from the 19th century to the 21st century. *Journal of Polymer Science Part A Polymer Chemistry* **2004**, *42* (3), 578-586.

[24] Simoneit, B. R. T.; Medeiros, P. M.; Didyk, B. M. Combustion Products of Plastics as Indicators for Refuse Burning in the Atmosphere. *Environmental Science & Technology* **2005**, *39* (18), 6961-6970.

[25] Block, C.; Van Caneghem, J.; Van Brecht, A.; Wauters, G.; Vandecasteele, C. Incineration of Hazardous Waste: A Sustainable Process? *Waste and Biomass Valorization* **2015**, *6* (2), 137-145.

[26] Zhao, H.; Wang, J. Chemical-looping combustion of plastic wastes for in situ inhibition of dioxins. *Combustion and Flame* **2018**, *191*, 9-18.

[27] Wiedinmyer, C.; Yokelson, R. J.; Gullett, B. K. Global emissions of trace gases, particulate matter, and hazardous air pollutants from open burning of domestic waste. *Environmental Science and Technology* **2014**, *48* (16), 9523-9530.

[28] Fahy, R. F.; LeBlanc, P. R.; Molis, J. L. Firefighter fatalities in the United States-2011; NFPA Emmitsburg, MD, 2012.

[29] Socha, A.; Abernethy, S.; Birmingham, B.; Bloxam, R.; Fleming, S.; McLaughlin, D.; Spry, D.; Dobroff, F.; Cornaccio, L. Plastimet Inc. fire in Hamilton, Ontario, July 9-12, 1997. **1997**.

[30] Fernando, S.; Jobst, K. J.; Taguchi, V. Y.; Helm, P. A.; Reiner, E. J.; McCarry, B. E. Identification of the Halogenated Compounds Resulting from the 1997 Plastimet Inc. Fire in Hamilton, Ontario, using Comprehensive Two-Dimensional Gas Chromatography and

(Ultra)High Resolution Mass Spectrometry. *Environmental Science & Technology* **2014**, *48* (18), 10656-10663.

[31] Tue, N. M.; Goto, A.; Takahashi, S.; Itai, T.; Asante, K. A.; Nomiyama, K.; Tanabe, S.; Kunisue, T. Soil contamination by halogenated polycyclic aromatic hydrocarbons from open burning of e-waste in Agbogbloshie (Accra, Ghana). *Journal of Material Cycles and Waste Management* **2017**, *19* (4), 1324-1332.

[32] Costa-Gómez, I.; Suarez-Suarez, M.; Moreno, J. M.; Moreno-Grau, S.; Negral, L.; Arroyo-Manzanares, N.; López-García, I.; Peñalver, R. A novel application of thermogravimetry-mass spectrometry for polystyrene quantification in the PM10 and PM2.5 fractions of airborne microplastics. *Science of the Total Environment* **2023**, *856*, 159041.

[33] Su, X.; Sutarlie, L.; Loh, X. J. Sensors and analytical technologies for air quality: particulate matters and bioaerosols. *Chemistry - An Asian Journal* **2020**, *15* (24), 4241-4255.

[34] ISBN, W. H. O. Ambient air pollution: A global assessment of exposure and burden of disease. **2016**.

[35] Grahame, T. J.; Schlesinger, R. B. Health Effects of Airborne Particulate Matter: Do We Know Enough to Consider Regulating Specific Particle Types or Sources? *Inhalation Toxicology* **2007**, *19* (6-7), 457-481.

[36] Hayward, S. J.; Gouin, T.; Wania, F. Comparison of Four Active and Passive Sampling Techniques for Pesticides in Air. *Environmental Science & Technology* **2010**, *44* (9), 3410-3416.

[37] Azari, A.; Vanoirbeek, J. A. J.; Van Belleghem, F.; Vleeschouwers, B.; Hoet, P. H. M.; Ghosh, M. Sampling strategies and analytical techniques for assessment of airborne micro and nano plastics. *Environment International* **2023**, *174*, 107885.

[38] Newton, G.; Raabe, O.; Mokler, B. Cascade impactor design and performance. *Journal of Aerosol science* **1977**, *8* (5), 339-347.

[39] Dunbar, C.; Mitchell, J. Analysis of cascade impactor mass distributions. *Journal of Aerosol Medicine* **2005**, *18* (4), 439-451.

[40] Wang, F. C.-Y. Polymer additive analysis by pyrolysis–gas chromatography: I. Plasticizers. *Journal of Chromatography A* **2000**, *883* (1), 199-210.

[41] Dzidic, I.; Carroll, D. I.; Stillwell, R. N.; Horning, E. C. Comparison of positive ions formed in nickel-63 and corona discharge ion sources using nitrogen, argon, isobutane, ammonia and nitric oxide as reagents in atmospheric pressure ionization mass spectrometry. *Analytical Chemistry* **1976**, *48* (12), 1763-1768.

[42] Mottaleb, M. A.; Sarker, S. D. Accelerated solvent extraction for natural products isolation. *Methods in Molecular Biology* **2012**, *864*, 75-87.

[43] Rodríguez-Solana, R.; Salgado, J. M.; Domínguez, J. M.; Cortés-Diéguez, S. Characterization of fennel extracts and quantification of estragole: Optimization and comparison of accelerated solvent extraction and Soxhlet techniques. *Industrial Crops and Products* **2014**, *52*, 528-536.

[44] Richter, B. E.; Jones, B. A.; Ezzell, J. L.; Porter, N. L.; Avdalovic, N.; Pohl, C. Accelerated Solvent Extraction: A Technique for Sample Preparation. *Analytical Chemistry* **1996**, *68* (6), 1033-1039.

[45] Lou, X.; Janssen, H.-G.; Cramers, C. A. Parameters Affecting the Accelerated Solvent Extraction of Polymeric Samples. *Analytical Chemistry* **1997**, *69* (8), 1598-1603.

[46] Giergielewicz-Możajska, H.; Dąbrowski, Ł.; Namieśnik, J. Accelerated Solvent Extraction (ASE) in the Analysis of Environmental Solid Samples — Some Aspects of Theory and Practice. *Critical Reviews in Analytical Chemistry* **2001**, *31* (3), 149-165.

[47] Alexandrou, N.; Smith, M.; Park, R.; Lumb, K.; Brice, K. The Extraction of Polycyclic Aromatic Hydrocarbons from Atmospheric Particulate Matter Samples by Accelerated Solvent Extraction (ASE). *International Journal of Environmental Analytical Chemistry* **2001**, *81* (4), 257-280.

[48] Wen, D.; Chen, Y.; Tong, Y.; Wang, H.; Zhang, H.; Luo, Y. Quantification of microplastics in soils using accelerated solvent extraction: comparison with a visual sorting method. *Bulletin of Environmental Contamination and Toxicology* **2021**, 1-8.

[49] Okoffo, E. D.; Ribeiro, F.; O'Brien, J. W.; O'Brien, S.; Tscharke, B. J.; Gallen, M.; Samanipour, S.; Mueller, J. F.; Thomas, K. V. Identification and quantification of selected plastics in biosolids by pressurized liquid extraction combined with double-shot pyrolysis gas chromatography–mass spectrometry. *Science of the Total Environment* **2020**, *715*, 136924.

[50] Ribeiro, F.; Okoffo, E. D.; O'Brien, J. W.; Fraissinet-Tachet, S.; O'Brien, S.; Gallen, M.; Samanipour, S.; Kaserzon, S.; Mueller, J. F.; Galloway, T.; et al. Quantitative Analysis of Selected Plastics in High-Commercial-Value Australian Seafood by Pyrolysis Gas Chromatography Mass Spectrometry. *Environmental Science & Technology* **2020**, *54* (15), 9408-9417.

[51] Ribeiro, F.; Okoffo, E. D.; O'Brien, J. W.; O'Brien, S.; Harris, J. M.; Samanipour, S.; Kaserzon, S.; Mueller, J. F.; Galloway, T.; Thomas, K. V. Out of sight but not out of mind: Size fractionation of plastics bioaccumulated by field deployed oysters. *Journal of Hazardous Materials Letters* **2021**, *2*, 100021.

[52] Yu, J. T.; Diamond, M. L.; Helm, P. A. A fit-for-purpose categorization scheme for microplastic morphologies. *Integrated Environmental Assessment and Management* **2023**, *19* (2), 422-435.

[53] Zhang, X.; Mell, A.; Li, F.; Thaysen, C.; Musselman, B.; Tice, J.; Vukovic, D.; Rochman, C.; Helm, P. A.; Jobst, K. J. Rapid fingerprinting of source and environmental microplastics using direct analysis in real time-high resolution mass spectrometry. *Analytica Chimica Acta* **2020**, *1100*, 107-117.

[54] Dierkes, G.; Lauschke, T.; Becher, S.; Schumacher, H.; Földi, C.; Ternes, T. Quantification of microplastics in environmental samples via pressurized liquid extraction and pyrolysis-gas chromatography. *Analytical and Bioanalytical Chemistry* **2019**, *411* (26), 6959-6968.

[55] Caldwell, J.; Taladriz-Blanco, P.; Lehner, R.; Lubskyy, A.; Ortuso, R. D.; Rothen-Rutishauser, B.; Petri-Fink, A. The micro-, submicron-, and nanoplastic hunt: A review of detection methods for plastic particles. *Chemosphere* **2022**, *293*, 133514.

[56] Morét-Ferguson, S.; Law, K. L.; Proskurowski, G.; Murphy, E. K.; Peacock, E. E.; Reddy, C. M. The size, mass, and composition of plastic debris in the western North Atlantic Ocean. *Marine Pollution Bulletin* **2010**, *60* (10), 1873-1878.

[57] Tiede, K.; Boxall, A. B. A.; Tear, S. P.; Lewis, J.; David, H.; Hassellöv, M. Detection and characterization of engineered nanoparticles in food and the environment. *Food Additives & Contaminants: Part A* **2008**, *25* (7), 795-821.

[58] Fraser, H. L.; Jones, I. P.; Loretto, M. H. Limiting factors in specimen thickness in conventional and scanning transmission electron microscopy. *The Philosophical Magazine: A Journal of Theoretical Experimental and Applied Physics* **1977**, *35* (1), 159-176.

[59] Primpke, S.; Lorenz, C.; Rascher-Friesenhausen, R.; Gerdts, G. An automated approach for microplastics analysis using focal plane array (FPA) FTIR microscopy and image analysis. *Analytical Methods* **2017**, *9* (9), 1499-1511.

[60] Caputo, F.; Vogel, R.; Savage, J.; Vella, G.; Law, A.; Della Camera, G.; Hannon, G.; Peacock, B.; Mehn, D.; Ponti, J.; et al. Measuring particle size distribution and mass concentration of nanoplastics and microplastics: addressing some analytical challenges in the sub-micron size range. *Journal of Colloid and Interface Science* **2021**, *588*, 401-417.

[61] Wagner, J.; Wang, Z.-M.; Ghosal, S.; Rochman, C.; Gassel, M.; Wall, S. Novel method for the extraction and identification of microplastics in ocean trawl and fish gut matrices. *Analytical Methods* **2017**, *9* (9), 1479-1490.

[62] Käppler, A.; Fischer, D.; Oberbeckmann, S.; Schernewski, G.; Labrenz, M.; Eichhorn, K.-J.; Voit, B. Analysis of environmental microplastics by vibrational microspectroscopy: FTIR, Raman or both? *Analytical and Bioanalytical Chemistry* **2016**, *408* (29), 8377-8391.

[63] Dümichen, E.; Eisentraut, P.; Bannick, C. G.; Barthel, A.-K.; Senz, R.; Braun, U. Fast identification of microplastics in complex environmental samples by a thermal degradation method. *Chemosphere* **2017**, *174*, 572-584.

[64] Kitahara, Y.; Takahashi, S.; Fujii, T. Thermal analysis of polyethylene glycol: Evolved gas analysis with ion attachment mass spectrometry. *Chemosphere* **2012**, *88* (5), 663-669.

[65] Ter Halle, A.; Jeanneau, L.; Martignac, M.; Jardé, E.; Pedrono, B.; Brach, L.; Gigault, J. Nanoplastic in the North Atlantic Subtropical Gyre. *Environmental Science & Technology* **2017**, *51* (23), 13689-13697.

[66] Akoueson, F.; Chbib, C.; Brémard, A.; Monchy, S.; Paul-Pont, I.; Doyen, P.; Dehaut, A.; Duflos, G. Identification of plastic additives: Py/TD-GC-HRMS method development and application on food containers. *Journal of Analytical and Applied Pyrolysis* **2022**, *168*, 105745.

[67] Ter Halle, A.; Jeanneau, L.; Martignac, M.; Jardé, E.; Pedrono, B.; Brach, L.; Gigault, J. Nanoplastic in the North Atlantic Subtropical Gyre. *Environmental Science & Technology* **2017**, *51* (23), 13689-13697.

[68] Dessì, C.; Okoffo, E. D.; O'Brien, J. W.; Gallen, M.; Samanipour, S.; Kaserzon, S.; Rauert, C.; Wang, X.; Thomas, K. V. Plastics contamination of store-bought rice. *Journal of Hazardous Materials* **2021**, *416*, 125778.

[69] Sullivan, G. L.; Gallardo, J. D.; Jones, E. W.; Hollliman, P. J.; Watson, T. M.; Sarp, S. Detection of trace sub-micron (nano) plastics in water samples using pyrolysis-gas chromatography time of flight mass spectrometry (PY-GCToF). *Chemosphere* **2020**, *249*, 126179.

[70] Duemichen, E.; Braun, U.; Senz, R.; Fabian, G.; Sturm, H. Assessment of a new method for the analysis of decomposition gases of polymers by a combining thermogravimetric solid-phase extraction and thermal desorption gas chromatography mass spectrometry. *Journal of Chromatography A* **2014**, *1354*, 117-128.

[71] Chun, S.; Muthu, M.; Gopal, J. Mass Spectrometry as an Analytical Tool for Detection of Microplastics in the Environment. *Chemosensors* **2022**, *10* (12), 530.

[72] Lin, Y.; Huang, X.; Liu, Q.; Lin, Z.; Jiang, G. Thermal fragmentation enhanced identification and quantification of polystyrene micro/nanoplastics in complex media. *Talanta* **2020**, *208*, 120478.

[73] Wampler, T. P. Pyrolysis-Gas Chromatography. Reference Module in Chemistry, Molecular Sciences and Chemical Engineering, Elsevier, 2014.

[74] Reichel, J.; Graßmann, J.; Letzel, T.; Drewes, J. E. Systematic Development of a Simultaneous Determination of Plastic Particle Identity and Adsorbed Organic Compounds by Thermodesorption–Pyrolysis GC/MS (TD-Pyr-GC/MS). *Molecules* **2020**, *25* (21), 4985.

[75] Skoog, D. A.; Holler, F. J.; Crouch, S. R. Principles of Instrumental Analysis. Thomson Brooks. **2007**.

[76] Kind, T.; Wohlgemuth, G.; Lee, D. Y.; Lu, Y.; Palazoglu, M.; Shahbaz, S.; Fiehn, O. FiehnLib: Mass Spectral and Retention Index Libraries for Metabolomics Based on Quadrupole and Time-of-Flight Gas Chromatography/Mass Spectrometry. *Analytical Chemistry* **2009**, *81* (24), 10038-10048.

[77] Li, X.; Dorman, F. L.; Helm, P. A.; Kleywegt, S.; Simpson, A.; Simpson, M. J.; Jobst, K. J. J. M. Nontargeted screening using gas chromatography–atmospheric pressure ionization mass spectrometry: recent trends and emerging potential. *Molecules* **2021**, *26* (22), 6911.

[78] Rennie, E. E.; Mayer, P. M. Confirmation of the "long-lived" tetra-nitrogen (N4) molecule using neutralization-reionization mass spectrometry and ab initio calculations. *The Journal of Chemical Physics* **2004**, *120* (22), 10561-10578.

[79] Kiontke, A.; Billig, S.; Birkemeyer, C. Response in Ambient Low Temperature Plasma Ionization Compared to Electrospray and Atmospheric Pressure Chemical Ionization for Mass Spectrometry. *International Journal of Analytical Chemistry* **2018**, *2018*, 5647536.

[80] Gross, J. H. W., Paul; Poole, C.; Townshend, A.; Miró, M. Mass Spectrometry | Electron Impact and Chemical Ionization. In Encyclopedia of Analytical Science (Third Edition), Academic Press, 2019; pp 334-343.

[81] Amiri, R.; Bissram, M. J.; Hashemihedeshi, M.; Dorman, F. L.; Megson, D.; Jobst, K. J. Differentiating Toxic and Nontoxic Tricresyl Phosphate Isomers Using Ion–Molecule Reactions with Oxygen. *Journal of the American Society for Mass Spectrometry* **2023**, *34* (4), 640-648.

[82] Gross, J. H. Tandem Mass Spectrometry. Springer International Publishing AG, 2017; pp 539-612.

[83] Fouquet, T.; Petersen, J.; Bomfim, J. A. S.; Bour, J.; Ziarelli, F.; Ruch, D.; Charles, L. Electrospray tandem mass spectrometry combined with authentic compound synthesis for structural characterization of an octamethylcyclotetrasiloxane plasma polymer. *International Journal of Mass Spectrometry* **2012**, *313*, 58-67.

[84] Polce, M. J.; Ocampo, M.; Quirk, R. P.; Wesdemiotis, C. Tandem Mass Spectrometry Characteristics of Silver-Cationized Polystyrenes: Backbone Degradation via Free Radical Chemistry. *Analytical Chemistry* **2008**, *80* (2), 347-354.

[85] Miller, P. E.; Denton, M. B. The quadrupole mass filter: Basic operating concepts. *Journal of Chemical Education* **1986**, *63* (7), 617.

[86] Glish, G. L.; Burinsky, D. J. Hybrid Mass Spectrometers for Tandem Mass Spectrometry. *Journal of the American Society for Mass Spectrometry* **2008**, *19* (2), 161-172.

[87] Giles, K.; Ujma, J.; Wildgoose, J.; Pringle, S.; Richardson, K.; Langridge, D.; Green, M. A Cyclic Ion Mobility-Mass Spectrometry System. *Analytical Chemistry* **2019**, *91* (13), 8564-8573.

[88] Kirk, A. T.; Bohnhorst, A.; Raddatz, C.-R.; Allers, M.; Zimmermann, S. Ultra-high-resolution ion mobility spectrometry—current instrumentation, limitations, and future developments. *Analytical and Bioanalytical Chemistry* **2019**, *411* (24), 6229-6246.

[89] Gabelica, V.; Marklund, E. Fundamentals of ion mobility spectrometry. *Current Opinion in Chemical Biology* **2018**, *42*, 51-59.

[90] Eldrid, C.; Ujma, J.; Kalfas, S.; Tomczyk, N.; Giles, K.; Morris, M.; Thalassinos, K. Gas Phase Stability of Protein Ions in a Cyclic Ion Mobility Spectrometry Traveling Wave Device. *Analytical Chemistry* **2019**, *91* (12), 7554-7561.

[91] Dodds, J. N.; Baker, E. S. Ion Mobility Spectrometry: Fundamental Concepts, Instrumentation, Applications, and the Road Ahead. *Journal of the American Society for Mass Spectrometry* **2019**, *30* (11), 2185-2195.

[92] Merenbloom, S. I.; Glaskin, R. S.; Henson, Z. B.; Clemmer, D. E. High-Resolution Ion Cyclotron Mobility Spectrometry. *Analytical Chemistry* **2009**, *81* (4), 1482-1487.

[93] Riches, E.; Palmer, M. E. Application of a novel cyclic ion mobility-mass spectrometer to the analysis of synthetic polymers: A preliminary evaluation. *Rapid Communications in Mass Spectrometry* **2020**, *34* (S2), e8710.

[94] Breen, J.; Hashemihedeshi, M.; Amiri, R.; Dorman, F. L.; Jobst, K. J. Unwrapping Wrap-around in Gas (or Liquid) Chromatographic Cyclic Ion Mobility–Mass Spectrometry. *Analytical Chemistry* **2022**, *94* (32), 11113-11117.

[95] Ujma, J.; Ropartz, D.; Giles, K.; Richardson, K.; Langridge, D.; Wildgoose, J.; Green, M.; Pringle, S. Cyclic Ion Mobility Mass Spectrometry Distinguishes Anomers and Open-Ring Forms of Pentasaccharides. *Journal of the American Society for Mass Spectrometry* **2019**, *30* (6), 1028-1037.

Chapter 2. Size-resolved identification and quantification of micro/nano-plastics in indoor air using pyrolysis gas chromatography-ion mobility mass spectrometry

Authors: Mahin Hashemihedeshi, Ethan Haywood, Daniel C. Gatch, Liisa Jantunen, Paul A. Helm, Miriam Diamond, Frank L. Dorman, Lindsay S. Cahill, Karl J. Jobst*

* Corresponding author

2.1. Abstract

Humans are likely exposed to micro-/nanoplastics (MNPs) through inhalation, but few studies have attempted to measure <1 µm MNPs in air, in part due to a paucity of analytical methods. Herein, we report on the development of an approach to identify and quantify MNPs in indoor air using a novel pyrolysis gas chromatographic cyclic ion mobility mass spectrometer (pyr-GCxcIM-MS). A variety of common plastic types were targeted, including polystyrene (PS), polyethylene (PE), polypropylene (PP), and polymethyl methacrylate (PMMA). The method was applied to size-resolved particulate (56 nm-18µm) collected from two different indoor environments, viz. a laboratory space and a private residence. Comprehensive two-dimensional separation by GCxcIM-MS also enabled the retrospective analysis of other polymers and plastic additives. The mean concentrations of MNP particles with diameters <10 µm and <2.5 µm in the laboratory were 47 ± 5 and 27 ± 4 µg/m³ respectively. In the private residence, the concentrations were 24 ± 3 and 16 ± 2 µg/m³. In both locations, PS was the most abundant MNP type. Approximately 57-67% of MNPs were characterized by particle diameters <2.5 µm, and 50-60% of the total particulate matter in the private residence was plastic. Non-targeted screening revealed the presence of plastic additives,

such as organophosphate esters whose abundance correlated with that of polyurethane (PU). This is consistent with their use as flame retardants in PU-based furniture and construction materials. The result of this study provides insight into the concentrations of MNPs in the indoor environment that underlines the critical need for further study of this route of exposure to MNPs and the plastics additives carried with them.

2.2. Introduction

Humans spend >90% of their time indoors [1]. They are likely exposed to microplastics (diameters <5 mm) [2, 3] and nanoplastics (diameters <1 μm) [4] predominantly by inhalation of indoor dust and ingestion of food contaminated by dust fall [5]. Aside from microplastics produced by the unintentional degradation of larger plastics, we are also exposed to microplastics produced for commercial purposes, including fibrous microplastics that leach from fabric in our clothing, furniture, and other everyday household items [6]. Young children are likely to be disproportionately exposed due to more frequent hand-to-mouth contact [7] with the floor and other surfaces where dust accumulates. Particles with diameters <10 μm are more likely to remain airborne and thus pose a greater risk of inhalation exposure. Nanoplastics are small enough to translocate from the lungs into the bloodstream [8], where they can accumulate in tissues and organs [9, 10]. There is mounting evidence that these exposures can potentially cause adverse respiratory effects, including lung cancer [11]. Despite these concerns, the occurrence of <10 μm microplastics and <1 μm nanoplastics in indoor air and their potential impact on human health remains unknown [6]. There are a limited number of studies that have attempted to measure microplastics indoors [12-15], and none have measured particle sizes <1 μm [16].

Research on nano*plastics* has been enabled by techniques that have long been employed for the characterization of inorganic nano*particles*. The morphology [17] of an environmental micro-/nanoplastic (MNPs) particle can be visually characterized by microscopy methods such as scanning electron microscopy-energy dispersive X-ray (SEM-EDX) [18], transmission electron microscopy (TEM) [19], atomic force microscopy (AFM) [20] and stimulated emission depletion (STED) [21] microscopy. To determine the size of MNPs, there are scattering methods such as dynamic light scattering (DLS) [22], asymmetric flow field-flow fractionation with multi-angle light scattering or total organic carbon (AF$_4$-MALS [23] or AF$_4$- TOC [24]) and nanoparticle tracking analysis (NTA) [25]. Spectroscopy methods utilized for chemical identification of MNPs include surface enhanced Raman (SERS) [26, 27], Raman tweezers [28, 29], Fourier transform infrared (FTIR) [30], X-ray photoelectron (XPS) [31] spectroscopy and photo induced forced microscopy (PiFM) [32]. While the above techniques can be useful for characterizing particles, they do have limitations. Typically, these techniques involve characterizing individual particles, as well as subjective visual assessments that are often restricted by particle size.

Mass spectrometry (MS) is an alternative technique used for identifying and quantifying the composition MNPs in complex samples. MS, in principle, is not limited to the size of the particle and can be combined with different techniques. Single particle inductively coupled plasma (SP-ICP) [33, 34] enables the quantification of the number of MNPs, but this requires functionalizing the nanoparticles with heavy metals, such as gold (Au) or holmium (Ho). Matrix-assisted laser desorption/ionization (MALDI) [35] is a powerful technique for the analysis of intact molecules with high molecular weights. This method can quantify plastic particles directly through MS. However, it cannot identify and quantify plastics and their additives simultaneously.

Most MS-based methods involve thermal decomposition methods, such as pyrolysis, or similar destructive techniques that target the products of decomposition. Pyrolysis can be performed in combination with ambient ionization techniques such as direct analysis in real time (DART) [36],[37] or following separation by gas chromatography (GC) [38] or liquid chromatography (LC) [39]. Wang et al. [39], used LC-MS to quantify the polymers polycarbonate (PC) and polyethylene terephthalate (PET) by depolymerization in sludge and indoor dust samples. Pyrolysis-gas chromatography (Pyr-GC) is a popular thermal decomposition method, which can provide structural information about the polymer changes, as well as insights into the presence of polymer additives. It has typically been coupled to single quadrupole MS [40, 41]. Recently tandem mass spectrometry (MS/MS) [42], and high-resolution time-of-flight (ToF) [43] platforms have also been hyphenated with pyr-GC, which can increase sensitivity, selectivity and enable the detection of a greater number of pyrolysis products that constitute an MNP's chemical fingerprint[36].

The present study reports on a method developed using pyrolysis-gas chromatography multiplexed with cyclic ion mobility mass spectrometry (Pyr-GCxcIM-MS). Ion mobility provides additional evidence that can strengthen the identification of the pyrolysis decomposition products. After elution through the GC, analyte molecules are transformed into ions, which travel through the mobility cell and their drift time is related to their size, shape and charge. The collision cross section (CCS), a unique identifier of an ion, can be determined from the measured drift time. The instrument also offers the capability of detecting thousands of chemical compounds, providing more detailed information on plastics and their additives than what can be obtained using standard pyr-GC-MS. This means that plastics and plastic additives can be identified without prior knowledge of their occurrence using an approach coined non-targeted screening [44, 45]. The

purpose of the present study is: (i) to develop a quantitative method for detecting common plastics in size-resolved particulate (ranging from 56 nm to 18 μm) by Pyr-GCxcIM-MS; (ii) to evaluate the effectiveness of soft ionization (APCI), tandem mass spectrometry, and ion mobility to identify plastics; and (iii) to apply the method to the indoor environment to demonstrate proof of concept that the concentration of MNPs can be determined simultaneously with the plastics additives.

2.3. Experimental

2.3.1. Chemical and Materials

Four different types of plastics, namely polymethyl methacrylate (PMMA), polypropylene (PP), polystyrene (PS), and polyethylene (PE), were selected as targets because they are among the most common plastics. A 25 mg/mL dispersion of PS nanoparticles (nominal size 50 nm) was purchased from Microsphere-Nanosphere (Cold Spring, NY, USA). PE, PP, and PMMA beads were obtained from Fisher Scientific (Hampton, New Hampshire, USA). The PE was used as received: the size of the microparticles ranged between 34-50 μm. The PMMA powder and PP granules were frozen with liquid Nitrogen, crushed using a mortar and pestle for 15 min, and separated using a 38 μm mesh stainless steel sieve. The glass fiber filters were obtained from Cole-Parmer (Quebec, Canada). Polyurethane foam (PUF) was purchased from Tisch Environmental Inc. (Village of Cleaves, OH) to confirm the identity of PUF detected by retrospective analysis of the GCxcIM-MS data. Likewise, the identity of TDCPP (tris(1,3-dichloro-2-propyl)phosphate) in the sample extracts was confirmed using a standard obtained from Wellington Laboratories (Guelph, ON, Canada).

2.3.2. Instrumental Analysis

Pyrolysis gas chromatographic cyclic ion mobility mass spectrometry (Pyr-GC-cIM-MS) experiments were performed using a Waters Cyclic IMS ion mobility mass spectrometer (Wilmslow, UK) coupled to an Agilent 8890 gas chromatograph (GC) using atmospheric pressure chemical ionization (APCI). Mass spectra were recorded between m/z 50 and 1200, enabling the detection of thousands of compounds released during thermal desorption and pyrolysis of the sample extracts. The GC inlet was equipped with a Gerstel CIS4 cooled injection system, thermal desorption unit and pyrolysis module. Automated injection of samples was achieved using a Gerstel Multipurpose-Sampler (MPS) Robotic autosampler. The analysis was performed in two steps: First, the TDU was initially set to desorb semi-volatile substances (SVOCs) such as plastics additives by ramping the temperature of the TDU from 50 to 320°C at a rate of 720 °C/min and then held for 10.43 min. The desorbed SVOCs are then swept by the helium (He) carrier gas through a heated transfer line (held at 350°C), the CIS4 (held at 320°C) and then focused on the head of the GC column (initially held at 50°C). Separation by GC was achieved using the oven program described below. Following the TDU analysis, the sample was re-injected and pyrolyzed by raising the temperature of the pyrolysis module to 500°C for 0.33 min with a follow-up time of 10 min at 320°C. The carrier gas used was He (99.999%) with a flow rate of 2 mL/min on column and a 40:1 split ratio at the CIS4 injector. The split valve on the TDU was closed for all experiments.

Analyte separation was performed with an Rtx-5 column (15 m × 0.25 mm × 0.25 μm). The initial oven temperature was set to 50°C, and then ramped to 320°C at 29 °C/min and held for 5 min. Nitrogen makeup flow of ~99.99% purity at 350 mL/min was used to sweep the GC eluent exiting the column through the ion volume. APCI was initiated by a corona discharge (3 μA) in positive ion mode. The source conditions were source temperature at 150°C, sampling cone at 40

V, extraction cone at 10 V, cone gas at 250 L/h, and auxiliary gas at 100 L/h. To internally correct the measured m/z in positive ion modes, column bleed ($C_9H_{27}O_5Si_5^+$ - m/z 355.0699) and background ions were used. The mass spectra were collected for m/z 50–1200. The cyclic ion mobility cell was operated in the single pass mode, with the separation time set to 2.0 ms and a traveling wave height of 15 V. Collision cross section (CCS) values were obtained by calibration with a set of 21 substances (aka, "major mix") supplied by Waters Corp. (Milford, MA).

2.3.3. Polymer Standard Preparation

The suspension of 50 nm PS particles was received in water (25 mg/mL). A 1 mL aliquot of the PS standard was reconstituted into DCM (25 mg/mL) [46]. Stock suspensions of PMMA, PP, and PE (25mg/mL) were made by dissolving <38 um sieved particles into Toluene. Stock solutions of PS, PMMA, PP, and PE were then diluted to 5 mg/mL and then combined to a suspension containing all four polymers at a concentration of 1 mg/mL in toluene. External calibration standards were prepared by adding 0.02 µg, 0.1 µg, 0.2 µg, 1 µg and 5 µg of each polymer onto a quartz glass bed inserted into a 40 µL quartz pyrolysis cup by serial dilution of the combined standard solution. The PS and PMMA are dissolved in toluene [47] at room temperature, but to promote dispersion/dissolution of PE [48] and PP [49, 50] during transfer steps, the stock solutions were heated to 120°C. The stock solution (25 mg/mL) of PUF was prepared by dissolving it in dimethylformamide (DMF) solvent at 80°C for 3 hours, employing a laboratory-grade magnetic stirrer.

2.3.4. Sampling Strategy

In this study, two indoor environments, namely a laboratory space and a home (both mechanically ventilated) were selected as sampling locations to evaluate the developed analytical method. Airborne particulate was collected using a Micro-Orifice Uniform Deposit Impactors (MOUDI) model 110 (MSP Corporation, Shoreview, MN, USA) for 72 hours. Eleven samples were collected at each site with corresponding cut point aerodynamic diameters: 0.056 µm, 0.10, 0.18, 0.32, 0.56, 1.0, 1.8, 3.2, 5.6, 10 and 18 µm. Glass fiber filters (Whatman GF/F) were used to collect sample particles, which were pre-cleaned in a muffle furnace at 450°C for 8 hours and then extracted in four cycles by accelerated solvent extraction using DCM. A PARTI5 Vacuum Pump (TSI Inc., USA) was used to draw air through the cascade impactor at a rate of 30 L/min for 72 hours at the height of 1.2 m, corresponding to the average adult breathing height.

2.3.5. Extraction of Samples

The filters were extracted using a Dionex ASE 350 Accelerated Solvent Extractor (Thermo Scientific, Germany) with a DCM solvent at a 100°C extraction temperature and 1500 psi pressure. DCM was chosen as the extraction solvent due to its ability to dissolve most polymers at high temperatures [51]. Each filter was loaded into a 10 mL stainless-steel extraction cell. Four cycles were performed on each extraction cell, using an 80% rinse volume, 250-second purge time, 9-second heating time, and 5-second static time. The resulting extract was collected in sample collection bottles, transferred to a 50 mL glass centrifuge tube, and concentrated under Nitrogen until the sample volume was reduced to approx. 1 mL. The sample extract was further reduced to 200 µL in a 2 mL GC vial.

2.3.6. Quality Assurance/Quality Control

The m/z and GC retention times of the pyrolysis decomposition products used for the quantitation of PS, PE, PP, and PMMA are summarized in Table 2.1. The accurate mass, isotope ratios and collision cross sections (CCSs) of all detected pyrolysis products fell within 5 ppm, -0.7 % and 1.7% of the theoretical or measured value obtained from an authentic standard. In order to evaluate whether the calculated similarity of the chromatogram is significant, we compared the pattern chromatogram pyrolyzed products of four different polymers in the sample and standard. The ratio between the abundance of the pyrolysis product used for quantification (Table 2.1) and selected qualifier decomposition products (Table 2.1) deviated <20%, which means the results of this ratio could be used for fingerprinting the results. All pyrolysis products reported herein were present at quantities that exceed the estimated method detection limits (MDL) by > 3-fold. MDLs were evaluated using 8 blank filters processed using the same steps as for the samples. The MDL was calculated by 3 times of standard deviations obtained from replicate (n = 8) measurements of filter blanks. For each set of 11 filters collected during a sampling event, one procedural blank was collected and analyzed. Polymer recovery samples (n=6) were prepared by fortifying the filters with 10 μg of PS, PE, PP, and PMMA, and then following the same extraction, and transfer steps used for all samples. Recovery, linearity and MDLs are reported in Table 2.2. Special care was taken during sample collection, pretreatment, and instrumental analysis to minimize potential contamination from the surrounding environment. Sample loading and drying procedures were carried out in a fume hood and nitrile gloves were worn during all steps. All glass sample containers were rinsed thoroughly with DCM before use.

2.3.7. Data Processing

The data were collected using Waters MassLynx 4.2 and quantitative analysis was performed using TargetLynx. In addition, GCxcIM-MS contour plots were generated using

DriftScope (v. 3.0). Progenesis QI was used to calculate the CCS and mass of each indicator in standard and sample (See Table 2.1).

2.4. Results and Discussion

2.4.1. Characterization of common polymers by pyr-GCxcIM-MS

The identification or classification of a polymer is based on the molecular composition of the products generated during thermal decomposition or pyrolysis. Figure 2.1 (A) displays the contour plot of retention time versus drift time, obtained for four different MNPs (PMMA, PP, PS, and PE) by pyr-GCxcIM-MS. Positive mode APCI was employed for this study, which involves ionization of the analyte molecule (M) through charge exchange with $N_2^{\bullet+}$ or $N_4^{\bullet+}$ radical cations generated by corona discharge. APCI is less energetic compared to EI. Consequently, spectra acquired using APCI display abundant molecular ions and little fragmentation [52].

The identification of polyethylene (PE) and polypropylene (PP) can be challenging because the pyrolysis of the two polymers leads to the formation of hydrocarbons that possess identical elemental composition. Harata et al. [52] demonstrated the use of Py-GC-APCI for characterizing PE/PP mixtures in a complex mixture. They observed that under APCI conditions, $[M+NO]^+$ adducts, and fragments generated therefrom, could be used to distinguish PE and PP. In the present study, a lower pyrolysis temperature (500°C vs 600°C) was used, and it was observed that higher molecular weight PE and PP decomposition products could be separated by both GC and ion mobility.

The pyrogram obtained from PP is displayed in Figure 2.1 B. Upon degradation, PP forms a wide range of branched and unsaturated hydrocarbons with the general formula C_xH_{2x-2}, containing between 25 and 52 carbon atoms. The m/z 600.6573 ion $C_{43}H_{84}$ was selected for quantification because of its high relative abundance. (Both quantification and qualifier ions are summarized in Table 2.1). Its mass spectrum is dominated by the molecular ion ($M^{\bullet+}$), and upon collision-induced dissociation (CID), see Figure 2.1 (D), it decomposes by loss of a methyl as well as cleavages along the backbone: the 42 Da spacing between peaks is characteristic of the - $CH_2CH(CH_3)$- repeating unit in PP. The pyrogram of PE (Figure 2.1 D) is also dominated by hydrocarbons with the general formula C_xH_{2x-2}, ranging from C_{21} to C_{42}. Like PP, the APCI mass spectra of the PE pyrolysis products were dominated by the molecular ion [52]. However, the pyrolysis products of PE could easily be distinguished from those of PP because (i) the CID mass spectrum of PE was characterized by fragment ions spaced 14 Da apart, consistent with its -CH_2- repeating units; (ii) the linear hydrocarbons generated from PE elute with a later retention time (RT) than the branched hydrocarbons generated by PP; and (iii) the linear hydrocarbons were characterized by larger CCSs than those of the branched hydrocarbons. Table 2.1 summarizes the m/z, RT and CCS measurements of the indicator compounds used in this study.

PS (Figure 2.1 C) pyrolyzes into the styrene trimer (m/z 312.1878), which was the dominant compound, with styrene dimer (m/z 208.1252) following behind. In source fragmentation of the trimer ion produces an intense m/z 207.1174 ion that was used for quantification. The pyrogram of PMMA (Figure 2.1 E), displayed pyrolysis products ranging from C_{19} to C_{34}. These products are associated with tetramer to heptamer molecules after the loss of the methoxy group. The mass spectra of the PS trimer ions (Figure 2.2 A) and the PMMA pentamer ions (Figure 2.2 B) display dissociation products that are consistent with their proposed structures.
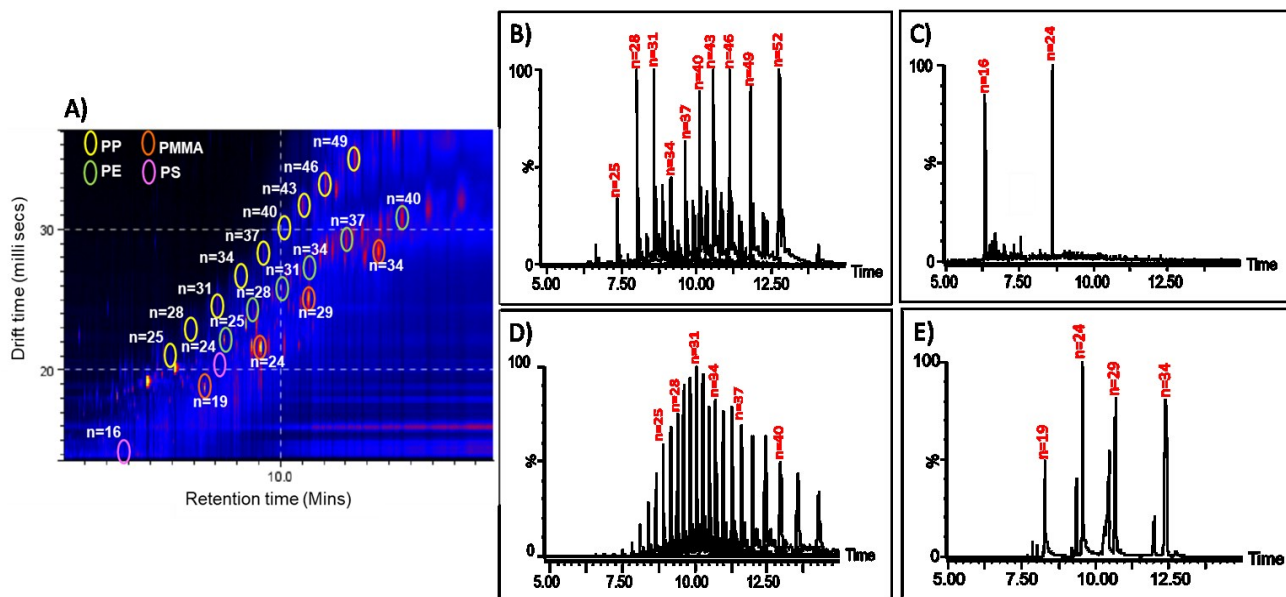
Figure 2.1. A) Retention time vs drift time contour plot of PP (yellow), PE (green),

PMMA (orange) and PS (pink); Extracted ion chromatograms of the decomposition products of

B) PP, C) PS, D) PE, and E) PMMA; Note: "n" refers to the number of carbons in the polymer

decomposition product's structure.
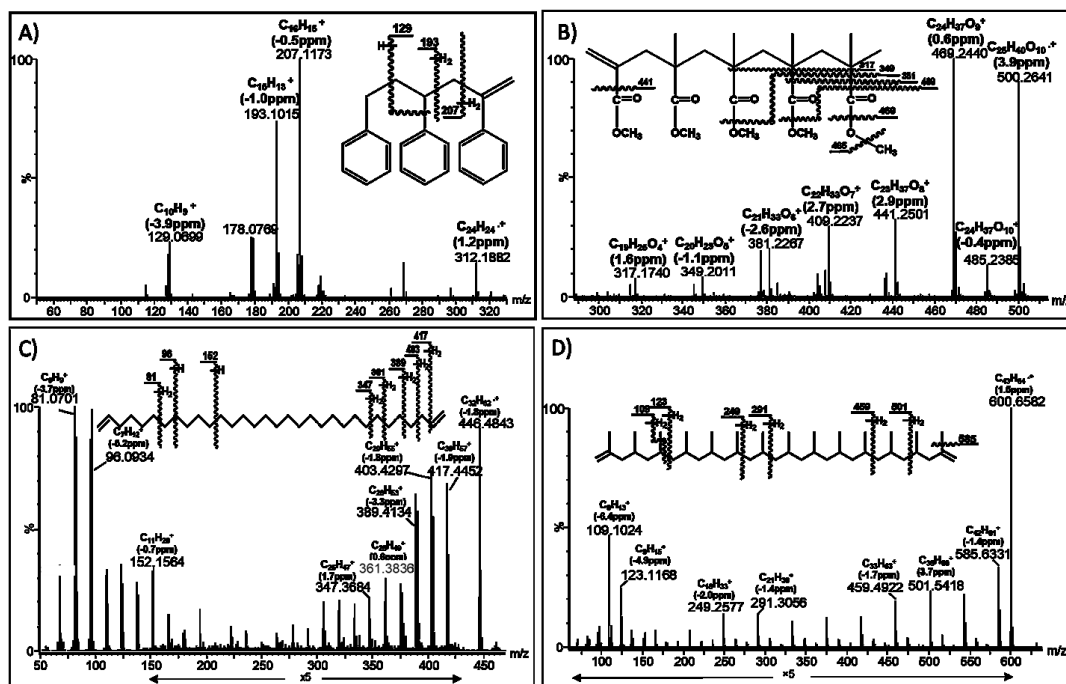
Figure 2.2. CID mass spectra of: A) the m/z 312 ions generated by the trimer of PS; B) the m/z 500 ions generated by the pentamer of PMMA; C) the m/z 446 ions generated by the $C_{32}H_{62}$ decomposition product of PE; D) and the m/z 600 ions generated by the $C_{43}H_{84}$ decomposition product of PP. Note: The collision energy was 12V for PS and 20V for PMMA, PE and PP is 20V.

Table 2.1. Summary of pyrolysis products generated from selected polymers and their m/z and CCS measurements. The elemental compositions highlighted in bold correspond to quantification ions, whereas the remaining ions were used as qualifiers.

Polymer	Particle size	Indicator ion formula	Retention time(min)	Exact Mass	m/z	Mass Error (ppm)	CCS	CCS dev. (%)
PS	50 (nm)	$C_{16}H_{15}$	7.69	207.1174	207.1168	-2.9	143.4	0.0
		$C_{16}H_{16}$	5.46	208.1252	208.1255	1.4	147.1	0.9
		$C_{24}H_{24}$	7.68	312.1878	312.1879	0.3	180.3	0.8
PMMA	<38 (µm)	$C_{19}H_{29}O_{7}$	7.43	369.1913	369.1919	1.6	177.7	0.0
		$C_{24}H_{37}O_{9}$	**8.72**	**469.2437**	**469.2448**	**2.3**	**200.2**	**-0.7**
		$C_{29}H_{45}O_{11}$	9.79	569.2962	569.2972	1.8	224.4	0.0
		$C_{34}H_{53}O_{13}$	10.77	669.3486	669.3500	2.1	247.5	0.5
PP	<38 (µm)	$C_{31}H_{60}$	7.72	432.4695	432.4693	-0.5	224.8	1.6
		$C_{34}H_{66}$	8.26	474.5164	474.5169	1.1	236.0	1.4
		$C_{37}H_{72}$	8.76	516.5634	516.5639	1.0	245.0	1.8
		$C_{40}H_{78}$	9.23	558.6104	558.6111	1.3	253.9	2.1
		$C_{43}H_{84}$	**9.67**	**600.6573**	**600.6575**	**0.3**	**265.0**	**1.9**
		$C_{49}H_{96}$	10.47	684.7512	684.7517	0.7	284.2	2.3
PE	<38 (µm)	$C_{26}H_{50}$	8.04	362.3913	362.3906	-1.9	211.1	1.2
		$C_{28}H_{54}$	8.53	390.4225	390.4221	-1.0	218.2	1.1
		$C_{32}H_{62}$	**9.41**	**446.4851**	**446.4855**	**0.9**	**232.9**	**0.9**
		$C_{34}H_{66}$	9.81	474.5163	474.5169	1.3	240.6	0.5
		$C_{37}H_{72}$	10.37	516.5631	516.5640	1.7	250.0	0.9
		$C_{40}H_{78}$	11.05	558.6104	558.6110	1.1	261.3	0.4
		$C_{43}H_{84}$	12.08	600.6573	600.6576	0.5	270.1	0.7

2.4.2. Method performance

The results of the pyr-GC/MS measurement of four standard polymers, PE (polyethylene), PP (polypropylene), PMMA (polymethyl methacrylate), and PS (polystyrene), indicated linear

50

calibration curves within the ranges of 0.1-5 µg for PE, PP, and PMMA and 0.2-5 µg for PS. The determination coefficients, represented by R^2, were all ≥ 0.98 (Table 2.2). Commercial PS nanospheres with a particle size of 50 nm and <38µm of PMMA, PE, and PP were used for evaluating their recoveries. It was found that the recovery of spiked plastic was 113 ± 19, 95 ± 25, 61 ± 29, and $114 \pm 23\%$ of PE, PP, PMMA, and PS, respectively (Table 2.2). Method detection limits (MDLs) were determined by replicate (n=8) measurements of blank filters. From the average relative responses, the standard deviation (SD) of blank polymer concentrations with the one-sided confidence interval was calculated, and three times SD was assumed as the MDL. The obtained MDLs are shown in Table 2.2, ranging from 0.005-0.41 µg/m^3.

Table 2.2. Performance characteristics of the method.

Polymer	Linear range (µg)	Linearity (R^2)	Recovery (n=6)	MDL (µg.m^{-3}) (n=8)
PE	0.2-5	0.994	113±19	0.040
PP	0.1-5	0.992	95±25	0.12
PMMA	0.1-5	0.998	61±29	0.005
PS	0.2-5	0.984	114±23	0.41

2.4.3. Quantitative analysis of PS, PMMA, PP and PE in indoor

air

The concentrations of MNPs made of polypropylene (PP), polyethylene (PE), polymethyl methacrylate (PMMA), and polystyrene (PS) were determined in air samples collected from two indoor locations: a laboratory space, and a private residence. The quantity of each polymer present at each stage of the cascade impactor was determined using an external calibration curve. The concentration of plastic particles in the air was calculated using the measured flow of air through the cascade impactor and the time during the sampler was deployed. The sampling process was carried out over 72 hours, during which 30 L/min of air was sampled, resulting in a total volume of 129,600 L or 129.6 m^3 of air. The quantitative results are presented in Figure 2.3, which displays the concentrations of plastics varying by particle size. Our findings indicate that the concentrations of MNP particles in the lab environment were comparable to those measured in the private residence; and most measurements exceeded the reported MDLs.
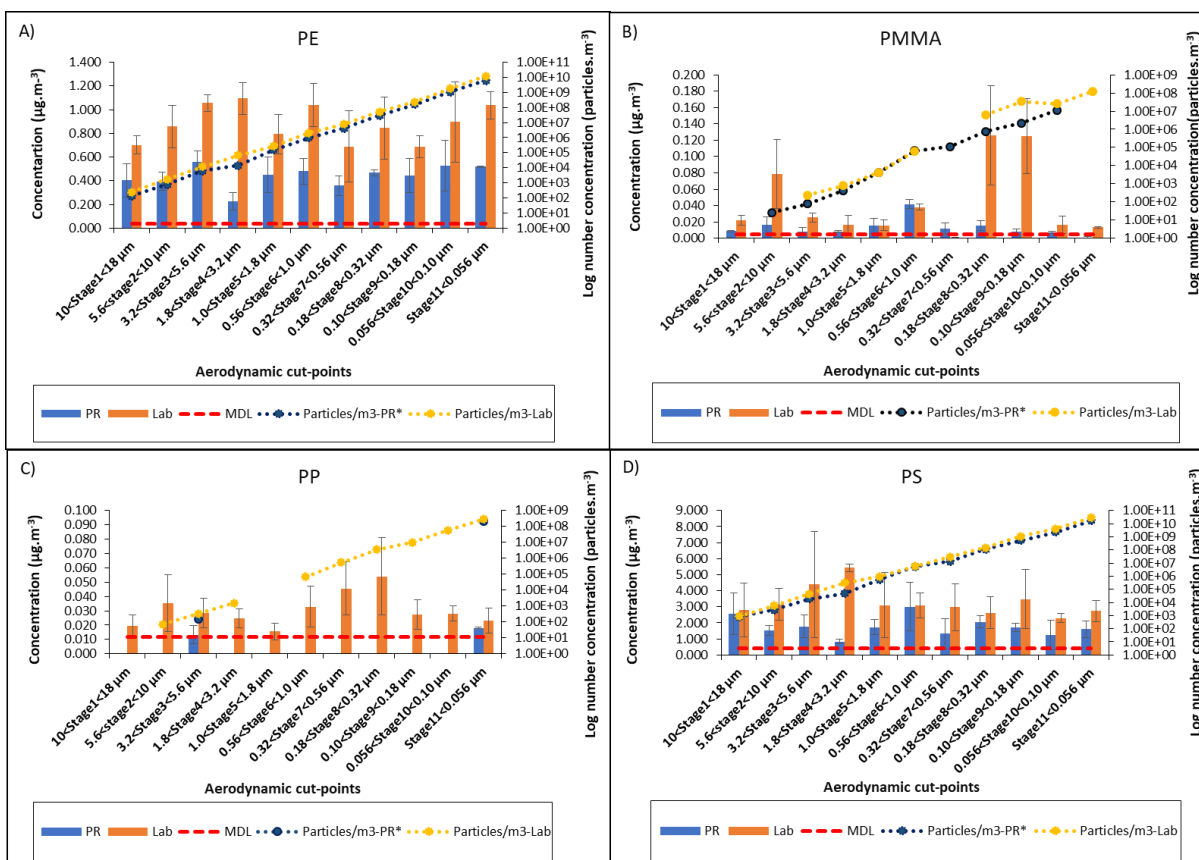
Figure 2.3. The concentrations ($\mu g/m^3$) of polymers A) PE, B) PMMA, C) PP and D) PS obtained from different aerodynamic cut-points (Note: PR* = Private residence). The error bars represent standard deviations of triplicate measurements.

Assessing the impact of MNPs as indoor air pollutants requires measuring not only mass concentration but also the number concentration (particles/m^3). The particle sizes of each sample were estimated based on the aerodynamic cut-point size of each stage of the cascade impactor. The polymer densities of PMMA, PP, PE, and PS were assumed to be 1.18, 0.91, 1.05 and 0.95 g/cm^3, respectively [41]. One limitation of this assumption is the fact that some polymers, such as high impact polystyrene or expanded polystyrene foam, are manufactured with a range of densities (0.03 to 1.25 g/cm^3). Thus, the particle concentration of PS below represents a conservative estimate. We assumed that all particles are spherical to simplify the analysis of number

concentration, which is a limitation of the present study. Further, the study by Liu et al. [53] suggests that inter-stage loss of nanoparticles may occur between the inlet and one of the lower stages, ranging between 2.9 and 26.1%. Equation 2.1 [41] was used to estimate the number concentrations (particles/m^3) of different MNPs in the lab and private residence are shown on the secondary axes of Figure 2.3.

$$C_n = {6C_m}\big/{\pi\rho d^3} \quad (2.1)$$

C_n is for the particle concentration of MNPs (Particles/m^3), C_m represents the mass concentration of MNPs (µg/m^3), d stands for the diameter of plastic particles (For simplification in calculating number concentrations, it was assumed that all MNPs were spherical), and ρ signifies the density (g/cm^3) of the previously mentioned plastics. The particle concentration of PP, PE, PMMA and PS particles with diameters <18 um approached 2.8 × 10^8 PP particles/m^3, 1.2 × 10^{10} PE particles/m^3, 1.2 × 10^8 PMMA particles/m^3, and 2.8 × 10^{10} PS particles/m^3, respectively. In comparison, the number concentrations in the private residence were somewhat lower than those in the lab, up to 2.2 × 10^8 PP particles/m^3, 5.9 × 10^9 PE particles/m^3, 1.1 × 10^7 PMMA particles/m^3, and 1.6 × 10^{10} PS particles/m^3. In line with the trend observed by Dris et al. [54] for particles and fibers >50 µm, the results in Figure 2.3 show that the number of particles increases exponentially with decreasing size. This suggests that most of the particles inhaled at the two sampling sites are characterized by small diameters (<2.5 µm), which can penetrate deeper into the lungs.

As shown in Figure 2.4, the concentrations of airborne PM$_{10}$ in the lab and private residence samples were found to be 46.5 and 24.4 µg/m^3, respectively. The concentration of PM$_{2.5}$ in the lab and private residence samples was measured at 26.8 and 16.1 µg/m^3. The World Health Organization has set guideline concentrations for PM$_{10}$ and PM$_{2.5}$ at 15 µg/m^3 and 10 µg/m^3,

respectively, for outdoor air pollution. While guidelines for indoor $PM_{10}/PM_{2.5}$ exposure do not currently exist, it appears that the measured MNP concentrations are significant. A gravimetric analysis of the filters obtained from the private residence suggests that the total $PM_{10}/PM_{2.5}$ concentrations consist of approximately 50-60% plastic (Figure 2.4 A).

Interestingly, the most abundant plastic found was PS. As described above, the styrene trimer was used as an indicator. Trimer styrene could possibly originate from other polymers besides polystyrene (PS). For example, approximately 50% of car tires are made from various types of styrene-butadiene rubber (SBR), which may also pyrolyze to form the styrene trimer. Exchange of indoor air with outdoor air could possibly carry road dust contaminated with SBR into the lab or private residence. However, recent studies [55] have shown that the outdoor concentrations of PS, using the same styrene trimer indicator, are in the low ng/m^3, which is 1000-fold lower than the indoor concentrations measured in the present study. The low concentrations measured outdoors are unlikely to be responsible for the high concentration found in the lab and private residence samples. One possible explanation for the presence of PS in the laboratory could be due to the fact that it is a relatively new space occupied in September 2021, and a significant amount of the PS may have originated from expanded polystyrene (EPS) commonly used for packaging materials. Since EPS is light weight, it is more likely to remain airborne.
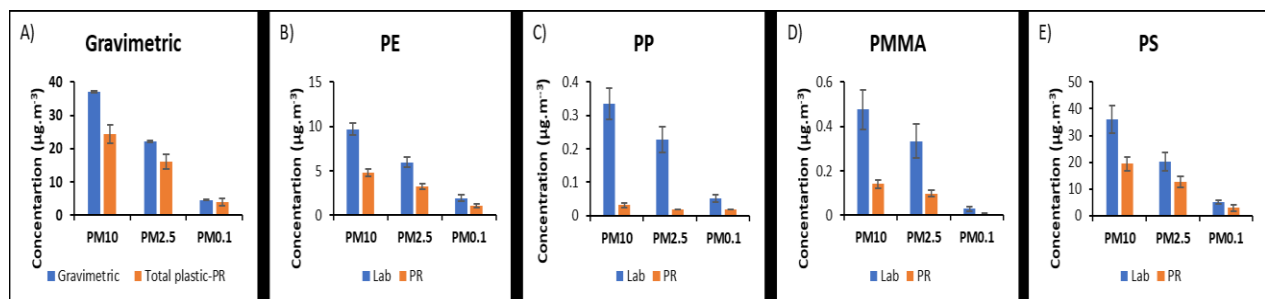
Figure 2.4. Concentrations of A) total $PM_{10}/PM_{2.5}$; as well as B) PE, C) PP, D) PMMA,

E) PS ($\mu g/m^3$) classified as either constituents of PM_{10}, $PM_{2.5}$, or $PM_{0.1}$. The error bars represent standard deviations of triplicate measurements.

2.4.4. Retrospective analysis of other polymers and plastic additives

The pyr-GCxcIM-MS used in the present study can detect thousands of chemical compounds in addition to the four polymers targeted for quantitation. For example, Figure 2.5 displays the extracted ion mobilogram (Figure 2.5 A), extracted ion chromatogram (Figure 2.5 C) and mass spectrum (Figure 2.5 E) of toluene diisocyanate (TDI), one of the products of the pyrolysis of an air sample extract. Aromatic diisocyanates are used in the production of foams and elastomers, including polyurethane foam PU [56]. PU is a versatile polymer used in applications such as flexible foam for bedding and furniture, carpet underlay, packaging, coatings, and adhesives. When an authentic sample of PU foam was dissolved in dimethylformamide [57] and pyrolyzed, we found that TDI is one of its decomposition products, and as shown in Figure 2.5 B, D and F, the retention time, mobility and mass spectrum of TDI matches those obtained from the indoor air sample.
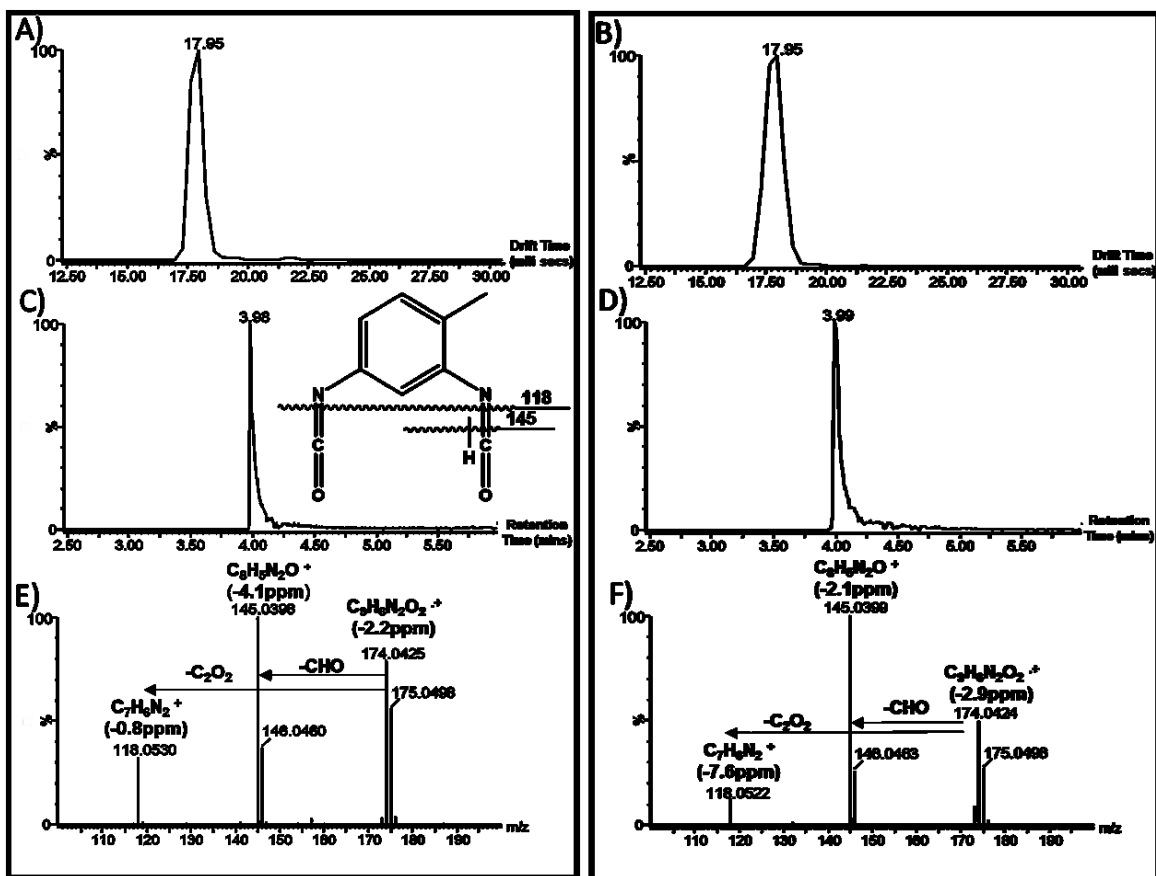
Figure 2.5. Drift time, chromatogram, and mass spectrum of polyurethane: A, C, E) Standard and B, D, F) Real sample, respectively.

MNPs, including PU foam, may serve as carriers of additives and small molecule pollutants, and inhalation of MNPs may be a source of exposure to these additives. It is expected that PU foam contains various flame retardants, including tris(1,3-dichloro-2-propyl) phosphate (TDCCP). Both PU and TDCPP were detected at all stages of the cascade impactor. If TDCPP were used as an additive flame retardant in PU foam, then one would expect a linear relationship between the concentrations of TDCPP and PU foam.

To investigate this, the concentration of TDCPP and PU were calculated at each stage of the cascade impactor using external calibration curves. Figure 2.6 A/B show that there is a

statistically significant positive correlation between the levels of TDCPP and PU in the lab (Pearson correlation coefficient = 0.85, p < 0.05). The results, see Figure 2.6 C, also showed that the concentration of TDCPP correlated with that of PP (Pearson correlation coefficient = 0.647, p < 0.05). In a review article published by S. Zhang [58], it was noted that there are various types of flame retardants used for polypropylene, including phosphate flame retardants. In contrast, see Figure 2.6 A, no correlation was observed for the other polymers (PMMA, PE, or PS). This suggests that the proposed method can provide an indication of the presence and contributions of tentatively identified compounds such as plastics additives using GCxcIM-MS.
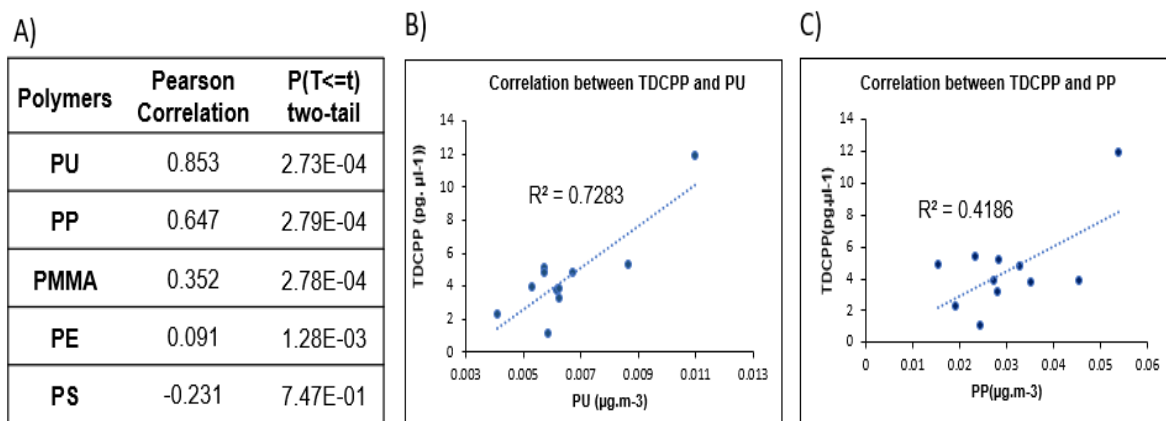
Figure 2.6. Correlation between TDCPP and polymers in the air sample

2.5. Conclusion

The present study reports on the development of a novel approach to identifying and quantifying PE, PP, PMMA and PS MNPs in indoor air. The results show that the mass concentrations of plastic particles smaller than 2.5µm are 27 ug/m^3 in a lab and 16 ug/m^3 in a private residence. These concentrations exceed those reported previously in the outdoor environment by 1000 fold [54], which suggests that the indoor environment may be an important

source of exposure to MNPs. Ion mobility offers the advantage of confirming the identities of pyrolysis products by their CCSs; along with the ability to simultaneously detect thousands of other compounds, including both polymers and small molecule pollutants, present in complex samples.

2.6. References

[1] Melymuk, L.; Demirtepe, H.; Jílková, S. R. Indoor dust and associated chemical exposures. *Current Opinion in Environmental Science Health* **2020**, *15*, 1-6.

[2] Thompson, R. C.; Olsen, Y.; Mitchell, R. P.; Davis, A.; Rowland, S. J.; John, A. W.; McGonigle, D.; Russell, A. E. Lost at sea: where is all the plastic? *Science* **2004**, *304* (5672), 838.

[3] Geyer, R.; Jambeck, J. R.; Law, K. L. Production, use, and fate of all plastics ever made. *Science Advances* **2017**, *3* (7), e1700782.

[4] Gigault, J.; Halle, A. T.; Baudrimont, M.; Pascal, P. Y.; Gauffre, F.; Phi, T. L.; El Hadri, H.; Grassl, B.; Reynaud, S. Current opinion: What is a nanoplastic? *Environmental Pollution* **2018**, *235*, 1030-1034.

[5] Zhang, Q.; Xu, E. G.; Li, J.; Chen, Q.; Ma, L.; Zeng, E. Y.; Shi, H. A Review of Microplastics in Table Salt, Drinking Water, and Air: Direct Human Exposure. *Environmental Science and Technology* **2020**, *54* (7), 3740-3751.

[6] Gasperi, J.; Wright, S. L.; Dris, R.; Collard, F.; Mandin, C.; Guerrouache, M.; Langlois, V.; Kelly, F. J.; Tassin, B. Microplastics in air: Are we breathing it in? *Current Opinion in Environmental Science Health* **2018**, *1*, 1-5.

[7] Stapleton, H. M.; Kelly, S. M.; Allen, J. G.; McClean, M. D.; Webster, T. F. Measurement of polybrominated diphenyl ethers on hand wipes: estimating exposure from hand-to-mouth contact. *Environmental Science and Technology* **2008**, *42* (9), 3329-3334.

[8] Mofijur, M.; Ahmed, S. F.; Rahman, S. M. A.; Arafat Siddiki, S. K. Y.; Islam, A. B. M. S.; Shahabuddin, M.; Ong, H. C.; Mahlia, T. M. I.; Djavanroodi, F.; Show, P. L. Source, distribution and emerging threat of micro- and nanoplastics to marine organism and human health: Socio-economic impact and management strategies. *Environmental Research* **2021**, *195*, 110857.

[9] Ragusa, A.; Svelato, A.; Santacroce, C.; Catalano, P.; Notarstefano, V.; Carnevali, O.; Papa, F.; Rongioletti, M.; Baiocco, F.; Draghi, S. Plasticenta: First Evidence of Microplastics in Human Placenta. Environment International. *Environment International* **2021**, *146*.

[10] Pauly, J. L.; Stegmeier, S. J.; Allaart, H. A.; Cheney, R. T.; Zhang, P. J.; Mayer, A. G.; Streck, R. J. Inhaled cellulosic and plastic fibers found in human lung tissue. *Journal of Cancer, Epidemiology Biomarkers & Prevention* **1998**, *7* (5), 419-428.

[11] Shi, Q.; Tang, J.; Liu, X.; Liu, R. Ultraviolet-induced photodegradation elevated the toxicity of polystyrene nanoplastics on human lung epithelial A549 cells. *Environmental Science: Nano* **2021**, *8* (9), 2660-2675.

[12] Liu, C.; Li, J.; Zhang, Y.; Wang, L.; Deng, J.; Gao, Y.; Yu, L.; Zhang, J.; Sun, H. Widespread distribution of PET and PC microplastics in dust in urban China and their estimated human exposure. *Environment International* **2019**, *128*, 116-124.

[13] Dris, R.; Gasperi, J.; Mirande, C.; Mandin, C.; Guerrouache, M.; Langlois, V.; Tassin, B. A first overview of textile fibers, including microplastics, in indoor and outdoor environments. *Environmental Pollution* **2017**, *221*, 453-458.

[14] Vianello, A.; Jensen, R. L.; Liu, L.; Vollertsen, J. Simulating human exposure to indoor airborne microplastics using a Breathing Thermal Manikin. *Scientific Reports* **2019**, *9* (1), 1-11.

[15] Zhang, J.; Wang, L.; Kannan, K. Microplastics in house dust from 12 countries and associated human exposure. *Environment International* **2020**, *134*, 105314.

[16] Huang, Y.; Qing, X.; Wang, W.; Han, G.; Wang, J. Mini-review on current studies of airborne microplastics: Analytical methods, occurrence, sources, fate and potential risk to human beings. *TRAC Trends in Analytical Chemistry* **2020**, *125*, 115821.

[17] Yu, J. T.; Diamond, M. L.; Helm, P. A. A fit-for-purpose categorization scheme for microplastic morphologies. *Integrated Environmental Assessment Management* **2023**, *19* (2), 422-435.

[18] Gniadek, M.; Dąbrowska, A. The marine nano-and microplastics characterisation by SEM-EDX: the potential of the method in comparison with various physical and chemical approaches. *Marine Pollution Bulletin* **2019**, *148*, 210-216.

[19] Lim, D.; Jeong, J.; Song, K. S.; Sung, J. H.; Oh, S. M.; Choi, J. Inhalation toxicity of polystyrene micro (nano) plastics using modified OECD TG 412. *Chemosphere* **2021**, *262*, 128330.

[20] Luo, H.; Xiang, Y.; Zhao, Y.; Li, Y.; Pan, X. Nanoscale infrared, thermal and mechanical properties of aged microplastics revealed by an atomic force microscopy coupled with infrared spectroscopy (AFM-IR) technique. *Science of the Total Environment* **2020**, *744*, 140944.

[21] Nguyen, B.; Tufenkji, N. Single-particle resolution fluorescence microscopy of nanoplastics. *Environmental Science and Technology* **2022**, *56* (10), 6426-6435.

[22] Enfrin, M.; Lee, J.; Gibert, Y.; Basheer, F.; Kong, L.; Dumée, L. F. Release of hazardous nanoplastic contaminants due to microplastics fragmentation under shear stress forces. *Journal of Hazardous Materials* **2020**, *384*, 121393.

[23] Battistini, B.; Petrucci, F.; Bocca, B. In-house validation of AF4-MALS-UV for polystyrene nanoplastic analysis. *Analytical Bioanalytical Chemistry* **2021**, *413*, 3027-3039.

[24] Mowla, M.; Shakiba, S.; Louie, S. M. Selective quantification of nanoplastics in environmental matrices by asymmetric flow field-flow fractionation with total organic carbon detection. *Chemical Communications* **2021**, *57* (96), 12940-12943.

[25] Lambert, S.; Wagner, M. Characterisation of nanoplastics during the degradation of polystyrene. *Chemosphere* **2016**, *145*, 265-268.

[26] Xu, G.; Cheng, H.; Jones, R.; Feng, Y.; Gong, K.; Li, K.; Fang, X.; Tahir, M. A.; Valev, V. K.; Zhang, L. Surface-enhanced Raman spectroscopy facilitates the detection of microplastics< 1 µm in the environment. *Environmental Science and Technology* **2020**, *54* (24), 15594-15603.

[27] Caldwell, J.; Taladriz-Blanco, P.; Rothen-Rutishauser, B.; Petri-Fink, A. Detection of sub-micro-and nanoplastic particles on gold nanoparticle-based substrates through surface-enhanced raman scattering (Sers) spectroscopy. *Nanomaterials* **2021**, *11* (5), 1149.

[28] Gillibert, R.; Balakrishnan, G.; Deshoules, Q.; Tardivel, M.; Magazzù, A.; Donato, M. G.; Maragò, O. M.; Lamy de La Chapelle, M.; Colas, F.; Lagarde, F. Raman tweezers for small microplastics and nanoplastics identification in seawater. *Environmental Science and Technology* **2019**, *53* (15), 9003-9013.

[29] Schwaferts, C.; Sogne, V.; Welz, R.; Meier, F.; Klein, T.; Niessner, R.; Elsner, M.; Ivleva, N. P. Nanoplastic analysis by online coupling of Raman microscopy and field-flow fractionation enabled by optical tweezers. *Analytical Chemistry* **2020**, *92* (8), 5813-5820.

[30] Li, Y.; Wang, Z.; Guan, B. Separation and identification of nanoplastics in tap water. *Environmental Research* **2022**, *204*, 112134.

[31] Hernandez, L. M.; Xu, E. G.; Larsson, H. C.; Tahara, R.; Maisuria, V. B.; Tufenkji, N. Plastic teabags release billions of microparticles and nanoparticles into tea. *Environmental Science and Technology* **2019**, *53* (21), 12300-12310.

[32] ten Have, I. C.; Duijndam, A. J.; Oord, R.; van Berlo-van den Broek, H. J.; Vollmer, I.; Weckhuysen, B. M.; Meirer, F. Photoinduced force microscopy as an efficient method towards the detection of nanoplastics. *Chemistry-Methods* **2021**, *1* (5), 205-209.

[33] Bolea-Fernandez, E.; Rua-Ibarz, A.; Velimirovic, M.; Tirez, K.; Vanhaecke, F. Detection of microplastics using inductively coupled plasma-mass spectrometry (ICP-MS) operated in single-event mode. *Journal of Analytical Atomic Spectrometry* **2020**, *35* (3), 455-460.

[34] Jiménez-Lamana, J.; Marigliano, L.; Allouche, J.; Grassl, B.; Szpunar, J.; Reynaud, S. A novel strategy for the detection and quantification of nanoplastics by single particle inductively coupled plasma mass spectrometry (ICP-MS). *Analytical Chemistry* **2020**, *92* (17), 11664-11672.

[35] Wu, P.; Tang, Y.; Cao, G.; Li, J.; Wang, S.; Chang, X.; Dang, M.; Jin, H.; Zheng, C.; Cai, Z. Determination of environmental micro (nano) plastics by matrix-assisted laser desorption/ionization–time-of-flight mass spectrometry. *Analytical Chemistry* **2020**, *92* (21), 14346-14356.

[36] Zhang, X.; Mell, A.; Li, F.; Thaysen, C.; Musselman, B.; Tice, J.; Vukovic, D.; Rochman, C.; Helm, P. A.; Jobst, K. J. Rapid fingerprinting of source and environmental microplastics using direct analysis in real time-high resolution mass spectrometry. *Analytica Chimica Acta* **2020**, *1100*, 107-117.

[37] Cody, R. B.; Fouquet, T. N.; Takei, C. Thermal desorption and pyrolysis direct analysis in real time mass spectrometry for qualitative characterization of polymers and polymer additives. *Rapid Communications in Mass Spectrometry* **2020**, *34*, e8687.

[38] Dümichen, E.; Eisentraut, P.; Bannick, C. G.; Barthel, A.-K.; Senz, R.; Braun, U. Fast identification of microplastics in complex environmental samples by a thermal degradation method. *Chemosphere* **2017**, *174*, 572-584.

[39] Wang, L.; Zhang, J.; Hou, S.; Sun, H. A simple method for quantifying polycarbonate and polyethylene terephthalate microplastics in environmental samples by liquid chromatography–tandem mass spectrometry. *Environmental Science Technology Letters* **2017**, *4* (12), 530-534.

[40] Leslie, H. A.; Van Velzen, M. J.; Brandsma, S. H.; Vethaak, A. D.; Garcia-Vallejo, J. J.; Lamoree, M. H. Discovery and quantification of plastic particle pollution in human blood. *Environment International* **2022**, *163*, 107199.

[41] Xu, Y.; Ou, Q.; Jiao, M.; Liu, G.; Van Der Hoek, J. P. Identification and quantification of nanoplastics in surface water and groundwater by pyrolysis gas chromatography–mass spectrometry. *Environmental Science and Technology* **2022**, *56* (8), 4988-4997.

[42] Luo, P.; Bai, M.; He, Q.; Peng, Z.; Wang, L.; Dong, C.; Qi, Z.; Zhang, W.; Zhang, Y.; Cai, Z. A Novel Strategy to Directly Quantify Polyethylene Microplastics in PM2.5 Based on Pyrolysis-Gas Chromatography–Tandem Mass Spectrometry. *Analytical Chemistry* **2023**, *95* (7), 3556-3562.

[43] Sullivan, G.; Gallardo, J. D.; Jones, E.; Hollliman, P.; Watson, T.; Sarp, S. Detection of trace sub-micron (nano) plastics in water samples using pyrolysis-gas chromatography time of flight mass spectrometry (PY-GCToF). *Chemosphere* **2020**, *249*, 126179.

[44] MacNeil, A.; Li, X.; Amiri, R.; Muir, D. C.; Simpson, A.; Simpson, M. J.; Dorman, F. L.; Jobst, K. J. Gas Chromatography-(Cyclic) Ion Mobility Mass Spectrometry: A Novel Platform for the Discovery of Unknown Per-/Polyfluoroalkyl Substances. *Analytical Chemistry* **2022**, *94* (31), 11096-11103.

[45] Steeves, K. L.; Bissram, M. J.; Kleywegt, S.; Stevens, D.; Dorman, F. L.; Simpson, A. J.; Simpson, M. J.; Cahill, L. S.; Jobst, K. J. Nontargeted screening reveals fluorotelomer ethoxylates in indoor dust and industrial wastewater. *Environment International* **2023**, *171*, 107634.

[46] Wang, Y.; Deng, R.; Yang, L.; Bain, C. D. Fabrication of monolayers of uniform polymeric particles by inkjet printing of monodisperse emulsions produced by microfluidics. *Lab on a Chip* **2019**, *19* (18), 3077-3085.

[47] Lau, W. W.; Burns, C. M.; Huang, R. Y. Compatibility of polystyrene and poly (methyl methacrylate) of various molecular weights in toluene. *Journal of Applied Polymer Science* **1984**, *29* (5), 1531-1536.

[48] Wong, S. L.; Ngadi, N.; Abdullah, T. Study on dissolution of low density polyethylene (LDPE). *Applied Mechanics and Materials* **2015**, *695*, 170-173.

[49] Iwamoto, S.; Yamamoto, S.; Lee, S.-H.; Endo, T. Mechanical properties of polypropylene composites reinforced by surface-coated microfibrillated cellulose. *Composites Part A: Applied Science Manufacturing* **2014**, *59*, 26-29.

[50] Cassano, D.; La Spina, R.; Ponti, J.; Bianchi, I.; Gilliland, D. Inorganic species-doped polypropylene nanoparticles for multifunctional detection. *ACS Applied Nano Materials* **2021**, *4* (2), 1551-1557.

[51] Hermabessiere, L.; Rochman, C. M. Microwave-Assisted Extraction for Quantification of Microplastics Using Pyrolysis–Gas Chromatography/Mass Spectrometry. *Environmental Toxicology Chemistry* **2021**, *40* (10), 2733-2741.

[52] Harata, K.; Kitagawa, S.; Iiguni, Y.; Ohtani, H. Identification of polymer species in a complex mixture by pyrolysis-gas chromatography-atmospheric pressure chemical ionization-high resolution time-of-flight mass spectrometry as a basis for environmental microplastic analysis. *Journal of Analytical Applied Pyrolysis* **2020**, *148*, 104828.

[53] Liu, C.-N.; Awasthi, A.; Hung, Y.-H.; Tsai, C.-J. Collection efficiency and interstage loss of nanoparticles in micro-orifice-based cascade impactors. *Atmospheric Environment* **2013**, *69*, 325-333.

[54] Dris, R.; Gasperi, J.; Mirande, C.; Mandin, C.; Guerrouache, M.; Langlois, V.; Tassin, B. A first overview of textile fibers, including microplastics, in indoor and outdoor environments. *Environmental Pollution* **2017**, *221*, 453-458.

[55] Costa-Gómez, I.; Suarez-Suarez, M.; Moreno, J. M.; Moreno-Grau, S.; Negral, L.; Arroyo-Manzanares, N.; López-García, I.; Peñalver, R. A novel application of thermogravimetry-mass spectrometry for polystyrene quantification in the PM10 and PM2.5 fractions of airborne microplastics. *Science of the Total Environment* **2023**, *856*, 159041.

[56] Coralli, I.; Goßmann, I.; Fabbri, D.; Scholz-Böttcher, B. M. Determination of polyurethanes within microplastics in complex environmental samples by analytical pyrolysis. *Analytical Bioanalytical Chemistry* **2023**, 1-15.

[57] Gonçalves, D.; Waddon, A.; Karasz, F. E.; Akcelrud, L. Conducting blends of soluble polyurethane and poly(o-methoxyaniline). *Synthetic Metals* **1995**, *74* (3), 197-199.

[58] Zhang, S.; Horrocks, A. R. A review of flame retardant polypropylene fibres. *Progress in Polymer Science* **2003**, *28* (11), 1517-1538.

Chapter 3. Differentiating toxic and non-toxic isomers of tetrachlorodibenzo-p-dioxin and chloro-polycyclic aromatic hydrocarbons by cyclic ion mobility mass spectrometry

3.1. Abstract

In 1997, a fire in Plastimet Inc. combusted about 400 tonnes of polyvinyl chloride (PVC). This fire led to the release of toxic compounds such as polymixed halogenated dioxins (PXDDs) into the environment. PXDDs are not only products that are generated through the combustion of plastic materials. Investigations on samples from Plastimet Inc. area confirmed the presence of other halogenated compounds, including halogenated polycyclic aromatic hydrocarbons (HPAHs). The study of HPAHs is challenging due to multiple isomeric compounds and limited availability of authentic standards. In this study, cyclic-ion mobility (cIM) technique was utilized to improve the separation of isomeric compounds from each other. The design of a cyclic ion mobility cell enables ions to undergo multiple passes, which can improve separation of isomers. First, toxic and non-toxic isomers of dioxin standards were differentiated through a multi-pass experiment. Then, data analysis techniques such as "unwrapping", and the conversion of the drift times to collision cross sections (CCS) were utilized to distinguish the dioxin like compound (2,3,6,7- tetrachloro anthracene (TCA)) in the sample from Plastimet area.

3.2. Introduction

Dioxins are a toxic group of persistent organic pollutants (POPs). The most toxic dioxin is 2,3,7,8-tetrachlorodibenzo-p-dioxin (TCDD) [1]. Exposure to TCDD has harmful consequences

on human health, such as cancer, neurological damage, and disruption of the reproductive, thyroid, and respiratory systems [2]. The risks of exposure to dioxins would be accelerated during the combustion of plastic waste. Plastic combustion increases health risks such as asthma and emphysema [3]. However, other dioxin-like compounds (DLCs) are also released during plastic combustion into the environment [4]. The group of hazardous chemicals, including poly mixed bromo/chloro dibenzo-p-dioxins and furans (PXDD and PADF), dioxin-like polychlorinated biphenyls (dl-PCB) [5], and halogenated PAHs (HPAHs) [6] share similar toxicity to TCDD due to their similar mechanism to stimulate the aryl hydrocarbon receptor (AhR). Persistence, slow elimination from the environment, and solubility in fat are common properties of these chemical compounds. These properties lead to their accumulation in fatty tissues through bioaccumulation and biomagnification [7]. However, due to differences in their ability to stimulate the receptor, these compounds require different doses to produce the same toxic effects [8, 9]. A study by Fernando [4] on soil samples from the Plastimet Inc. area revealed that the combustion of plastics released HPAHs in higher concentrations than dioxins. This result underscores the importance of investigating HPAHs [10]. Chloro-PAHs, such as 2,3,6,7-tetrachloroanthracene (2367-TCA) have a structure close to 2378-TCDD, resulting in similar toxicity [6]. TCA has multiple potential isomers, and it is important to identify toxic isomers accurately. To distinguish the most toxic isomers from others, using authentic standards or specific instruments for their separation and identification is required.

The separation of isomers is required due to their different physicochemical properties and distinct biological responses [11]. The study by Fernando et al. [12] proposed to differentiate PXDD toxic isomer by APCI in negative mode. They suggested APCI as an ionization technique in negative mode, enabling the detection of PXDD isomers through specific bond cleavage.

However, this method is impractical for other DLCs. Ion mobility spectrometry (IMS) [13-15] is a method that is capable of separating isomers. In IMS, ions will be separated based on their mobility in a chamber filled with the inert buffer gas along with an electrical field [16]. The mobility of ions is determined by their collision cross section (CCS). This CCS is calculated based on the average area of the ion interacting with a carrier gas and this property depends on their size and shape [17]. IM-MS provides rapid structural separation within milliseconds (ms), followed by identification through MS [18]. Cyclic ion mobility mass spectrometry (cIM-MS) is an advanced technique with increased resolution power [19, 20]. The details about instruments and geometry of cyclic cells have been explained by Giles et al. [21]. In brief, cIM-MS design allows for increasing the pass number of ions and extending the path length through the drift tube [20]. The cIM-MS assists in a non-targeted analysis and helps for characterization of unknown compounds as multi-dimensional techniques [22]. However, there is an issue during multi-pass experiments, known as wrap-around. Wrap-around happened when the faster ions over-take with slower ions and it is an important problem through the analysis of samples with complex matrix. Breen et al. [23] addressed this problem and proposed "unwrapping" data points that is explained in following experimental section.

The goal of this study was to develop a method to separate and distinguish toxic and non-toxic isomers. Multi-pass experiments were employed by cIM, both for dioxin standards and real samples. A data analysis method known as "unwrapping" was utilized. This method allowed to determine the number of passes for ions and then calculate their periodic drift times. Then, collision cross section (CCS) values were derived from converting periodic drift time to CCS using a standardized procedure. Through this research, the potential candidates of with higher toxicity were detected among the various isomeric compounds.

3.3. Experimental

3.3.1. Chemical and Materials

The soil sample preparation procedure is addressed by Myers et al. [24]. The sample used in their research originated from an archive of samples collected at the site of a fire in 1997 at Plastimet Inc., located in Hamilton, Ontario, Canada. Their study provided detailed information on the specific steps for sample preparation. The chemical standards including 1234, 1378, and 2378-TCDD were purchased from Wellington Laboratories (Guelph, Ontario). For analysis, one microliter portion of the obtained sample was introduced into a gas chromatography-cyclic ion mobility (GC-cIM-MS) system.

3.3.2. Instrumental Analysis

The experimental setup was a Waters Select Series Cyclic IMS ion mobility mass spectrometer (Wilmslow, UK) in conjunction with an Agilent 8890 Gas chromatograph employing atmospheric pressure chemical ionization (APCI). Analyte separation was accomplished using an Rtx-5HT column (15 m × 0.25 mm × 0.1 μm). In most cases, the experiments commenced with an initial oven temperature of 90°C for 1 min. The oven temperature was then increased at a rate of 27 °C/min until reaching 325°C, then maintained for 5.3 min. Standard solutions (with a volume of 1μL) were injected using the split-less mode. The inlet temperature was set to 280°C, and carrier gas, Helium (He), flow rate was set at 3 mL/min. Nitrogen (N_2) was a make-up with flow of approximately 350 mL/min, ensuring ~99.99% purity. For atmospheric pressure chemical ionization, solvent-free conditions were maintained, and corona discharge (with a current of 2 μA) was utilized in the positive mode. In positive mode, molecules underwent ionization through

charge exchange with $N_2^{\bullet+}$. The source conditions consisted of a source temperature of 150°C, a sampling cone voltage of 40 V, a cone gas flow rate of 175 L/hour, and an auxiliary gas flow rate of 100 L/hour. Mass spectra were acquired in the m/z range of 50 – 1200. To internally correct the measured m/z values, column bleed ($C_9H_{27}O_5Si_5^+$ - m/z 355.0699) was employed in positive mode. The cyclic ion mobility cell was operated with a separation time of 10.64 ms and a traveling wave height of 15 V. Multi-pass experiments were performed by extending the separation time to 389.14 ms, corresponding to 35 passes. Collision-induced dissociation (CID) experiments used Nitrogen as the collision gas with a collision energy of 6 V in the trap region and 4 V in the transfer region.

3.3.3. Data Processing

The data were collected using Waters MassLynx 4.2. In addition, GCxcIM-MS contour plots were generated using DriftScope (v.3.0).

3.4. Results and Discussion

3.4.1. Separation of Dioxin isomers with multi-pass experiment

The focus was on separating three dioxins: 2378-TCDD, 1378-TCDD, and 1234-TCDD. The close structures of 2378 and 1378 pose a challenge for separation since their collision cross sections (CCS) are expected to be close. The number of passes was increased in the experiment to 35 to address the resolution issue. In Figure 3.1, retention time versus drift time contour plot of three dioxins is shown. In a single-pass experiment, 2378-TCDD and 1378-TCDD aligned in a single line. However, by increasing the number of passes, those with lower CCS move fast, while compounds with higher CCS pass slowly. Among these three compounds, the drift times of 2378 and 1378 are closely aligned, while 1234 exhibits faster movement due to its lower CCS. These

results aligned with the order of the CCS values, which were calculated as 163.7 ± 2, 157.9 ± 0.9, and 160.93 ± 2 Å^2 using MobCal-MPI for 2378, 1234 and 1378- TCDD, respectively.
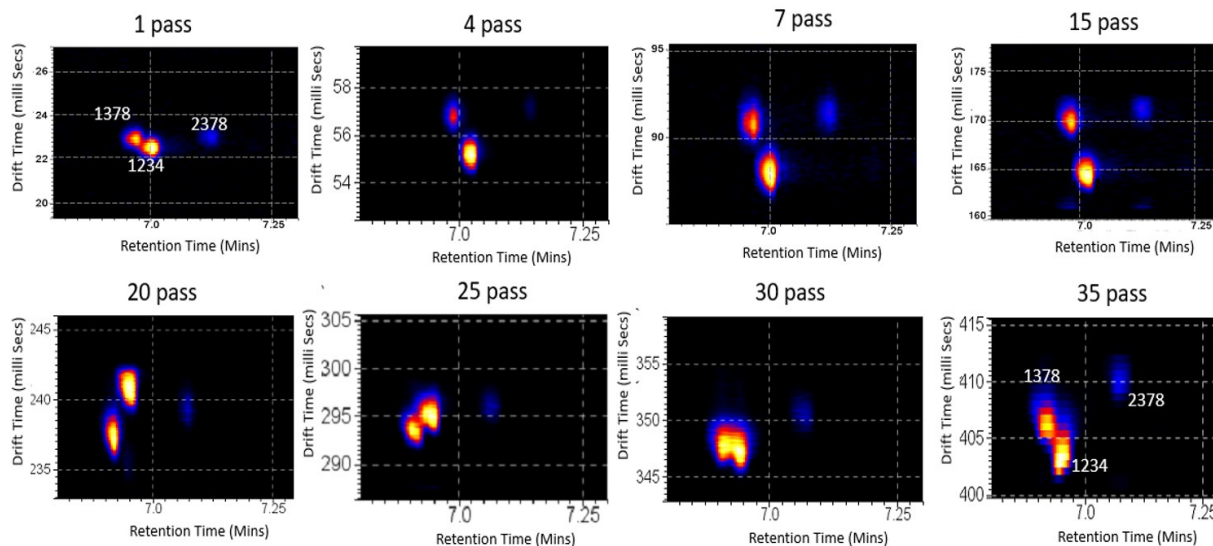
Figure 3.1. Multi-pass experiment for separation of 1378, 1234 and 2378-TCDD

In this process, the duration of an ion's travel through a cycle cell is referred to as periodic drift time (t_{1p}). Arrival time (t_a) is the time taken for ions to pass through the cyclic cell and traverse between the trap and the detector (Equation 3.1).

$$t_a = nt_{1p} + t_{0p} \quad (3.1)$$

The "t_{0p}", zero-pass time, is a time that it takes for ions to travel from the trap region to the detector, and "n" is the number of passes. The correlation between the arrival time and the number of passes is linear (Shown in Figure 3.2). The slopes of these diagrams represent the mean periodic drift time. The mean periodic drift times for 1378, 1234, and 2378-TCDD over 35 passes are 11.35 ± 0.02, 11.19 ± 0.06, and 11.25 ± 0.02 ms, respectively.

73
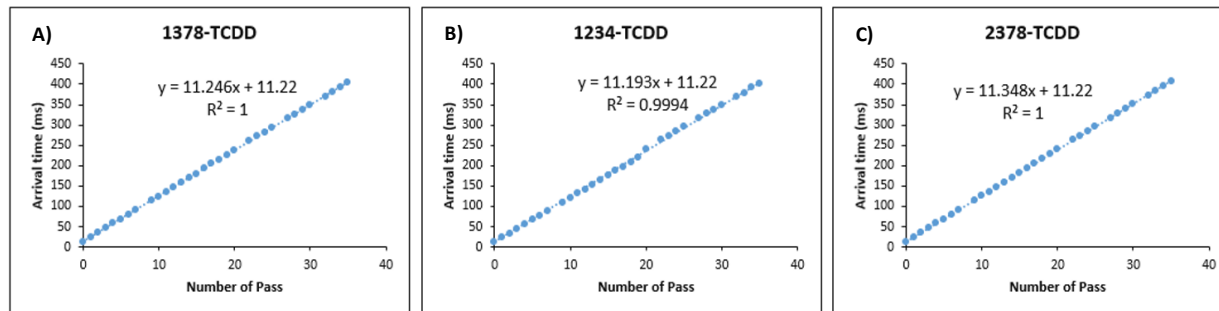
Figure 3.2. Diagram of correlation between arrival time (ms) and the number of passes A) 1378-TCDD, B) 1234-TCDD and C) 2378-TCDD

3.4.2. The wrapping and unwrapping result of HPAHs

In the analysis of archived sample, the initial step involved increasing the number of passes, which allowed the separation of TCA isomers. Figure 3.3 (A) illustrates after three passes and Figure 3.3 (B) indicates increasing the number of passes to 16-17. In Figure 3.3 (A), the Cl-TCA isomers (with elemental composition $C_{14}H_6Cl_4$) are partially resolved after 3 passes through the cyclic cell. When the number of passes increases (See Figure 3.3 B), the number of separable isomers increases from 11 to 17.

By employing a multi-pass experiment, interpretation of data becomes complicated. The wrapped data has inaccuracy in detecting the possible 2367-TCA compound. Unwrapping is beneficial for analysis of real samples containing complex matrices. Unwrapping involves calculating the periodic drift time and pass numbers for each individual compound. For calculating the periodic drift time, the zero pass and one pass experiment were employed. The zero pass in our experiment refers to a separation time of 0.01 ms, indicating that ions do not pass through the

mobility cell. In the one-pass experiment, the separation time is approximately 1-2 ms, allowing the compounds to undergo a single pass through the cyclic cell before reaching the detector.

As depicted in Figure 3.3 (C), the isomers exhibit different pass numbers. However, with the use of unwrapped data, the interpretation process becomes easier. In Figure 3.3 (A), the Cl-PAH isomers (with elemental composition $C_{14}H_6Cl_4$) are partially resolved after 3 passes through the cyclic cell. When the number of passes increases (See Figure 3.3 B), the number of separable isomers increases from 11 to 17. Even though not all compounds in (A) can be resolved, one can still use the unresolved drift time to extrapolate the number of passes, resulting in the "unwrapped" plot shown in panel (C).
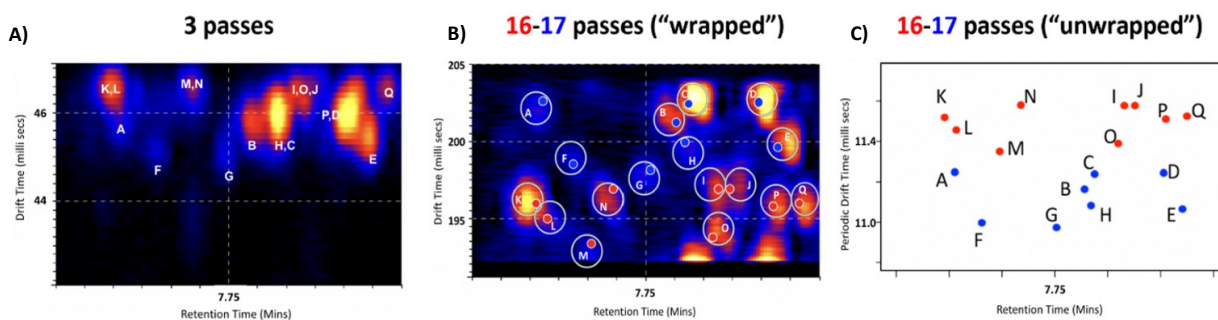
Figure 3.3. Contour plot displaying gas chromatography retention time vs drift time A) 3 passes, B) 16-17 passes, and C) diagram of retention time vs periodic drift time.

3.4.3. Application of CCS in differentiated toxic compound

Since CCS is unaffected by the matrix of the sample, it is a useful property for targeted and non-target experiments [25]. There are various methods for determining the CCS. One approach involves predicting the CCS for known compounds with known structures. Mesleh et al. [26] developed MobCal based on the kinetic theory of gases to compute the averaged cross sections.

75

However, while MobCal enables the prediction of CCS values, experimental methods also exist for CCS calculation. Ion mobility technique measurement is used to determine CCS. Ion mobility depends on the average collision cross section. A semi-linear relationship between CCS and drift time (shown in Equation 3.2) can be employed to calculate CCS (Ω) based on experimental data. Converting drift time (t_D) in seconds to collision cross section (CCS) in square meters (m^2), needs to have precise measurement of pressure (P) in torr and temperature (T) in Kelvin. Gabelica et al. [27] mentioned to the following equation that would be used specifically for a standard drift tube separator operating under a constant electric field:

$$\Omega = \frac{(18\pi)^{1/2}}{16} \frac{ze}{(k_b T)^{1/2}} \left(\frac{1}{m_I} + \frac{1}{m_N}\right)^{1/2} \frac{t_D E}{L} \frac{760}{P} \frac{T}{27.3} \frac{1}{N} \quad (3.2)$$

Here, "k_b" represents the Boltzmann constant, "z" denotes the ion charge, "e" is the elementary charge in Coulombs (C), "m_I" refers to the mass of the ion, "m_N" represents the mass of the neutral gas (both measured in kilograms, kg), "E" indicates the electric field strength in volts per meter (V/m), "L" represents the length of the drift region in meters (m), and "N" is the number density of the neutral gas in cubic meters (m^3). Some studies have described detailed procedures for making accurate CCS measurements using standard drift tubes [27]. However, it is important to note that calculating CCS using this equation relies on accurately measuring gas purity, pressure, and temperature. Due to the limitations in accurately measuring these factors, it is recommended to calibrate the drift time using ions with known CCS values.

A calibration method was established with the standards of a known compound that helps to identify compounds without authentic standards. The periodic drift time for each dioxin was obtained by analyzing the linear correlation in Figure 3.2. The slope of this graph represents the periodic drift time for three dioxins as known compounds. The average periodic drift times over

76

35 passes were found to be 11.35 ± 0.02 ms for 1378-TCDD, 11.19 ± 0.06 ms for 1234-TCDD, and 11.25 ± 0.02 ms for 2378-TCDD. For calibration purposes, it is necessary to have CCS values for known compounds. The CCS values for 1234-TCDD, 1378-TCDD, and 2378-TCDD were predicted using MobCal-MPI. The CCS need to be corrected (CCS′). The CCS′ was based on Equation 3.3 mentioned in the calibration protocol published by Ruotolo et al. [28]. In this equation, the correct CCS (Ω) was adjusted for both ion charge state and reduced mass (μ) to generate Ω'.

$$\Omega' = \frac{\Omega}{charge \times (1/\mu)^{1/2}} \quad (3.3)$$

Following the calculating of CCS′ (Equation 3.3), a plot of ln(CCS′) versus ln(t′$_D$) was generated. The t′$_D$ represents the corrected drift time (t′$_D$ obtained by subtracting $\frac{c\sqrt{m/z}}{1000}$ from t$_D$). The constant "c" is specific to each instrument and typically is in the range of 1.4 to 1.6. The subtraction term is negligible, accounting for <0.2% of t$_D$. Therefore, t$_D$ was used without subtracting this term.

The results obtained from this experimental phase demonstrated a linear relationship between ln Ω' and ln t$_D$ for the three dioxins, as described by the equation ln Ω' = 2.478 ln t$_D$ + 0.698 (R^2 > 0.97) (described by Equation 3.4).

$$ln\,\Omega' = X \times \ln t_D + \ln A \quad (3.4)$$

In the final step of the calibration process, it was necessary to apply a new correction to t$_D$ (based on Equation 3.5).

$$t'_D = t_D{}^X \times charge \times (1/\mu)^{1/2} \quad (3.5)$$

Following the application of this correction, the CCS was plotted against t'_D. This approach yields a linear calibration plot, establishing a direct relationship between the predicted CCS and drift time. This calibration curve employed to determine the CCS of unknown compounds. The periodic drift time (t_D) for TCA isomers is calculated by plotting the arrival time against the number of passes in a multi-pass experiment. By utilizing the equation and knowing the mean periodic drift time for each TCA isomer, the CCS for each isomer was calculated (Shown in Table 3.1). Additionally, the CCS for 2367-TCA, toxic isomer, is calculates by MobCal-MPI (153.8 ± 1.3 Å^2). Figure 3.4 (A) illustrates the separation of the TCA isomers through 16-17 passes. Figure 3.4 (B) presents the CCS values corresponding to each possible isomer. The results indicate that among 17 TCA isomers in this sample, two plausible candidates (H and E) exhibit CCS values close to that of 2367-TCA.

Table 3.1. Summary of TCA isomers' properties and characteristics

Compounds	Retention time (min)	Periodic drift time (ms)	Measured CCS (Å^2)
A	7.65	11.23	159.6
B	7.78	11.17	157.5
C	7.79	11.24	160.1
D	7.85	11.25	160.4
E	7.87	11.07	154.1
F	7.68	11.00	151.7
G	7.75	10.98	151.0
H	7.79	11.09	154.9
I	7.82	11.51	169.6
J	7.83	11.58	172.2
K	7.65	11.52	170.1
L	7.66	11.46	167.9
M	7.70	11.36	164.2
N	7.72	11.58	172.3
O	7.81	11.38	165.1
P	7.86	11.51	169.6
Q	7.89	11.52	170.1
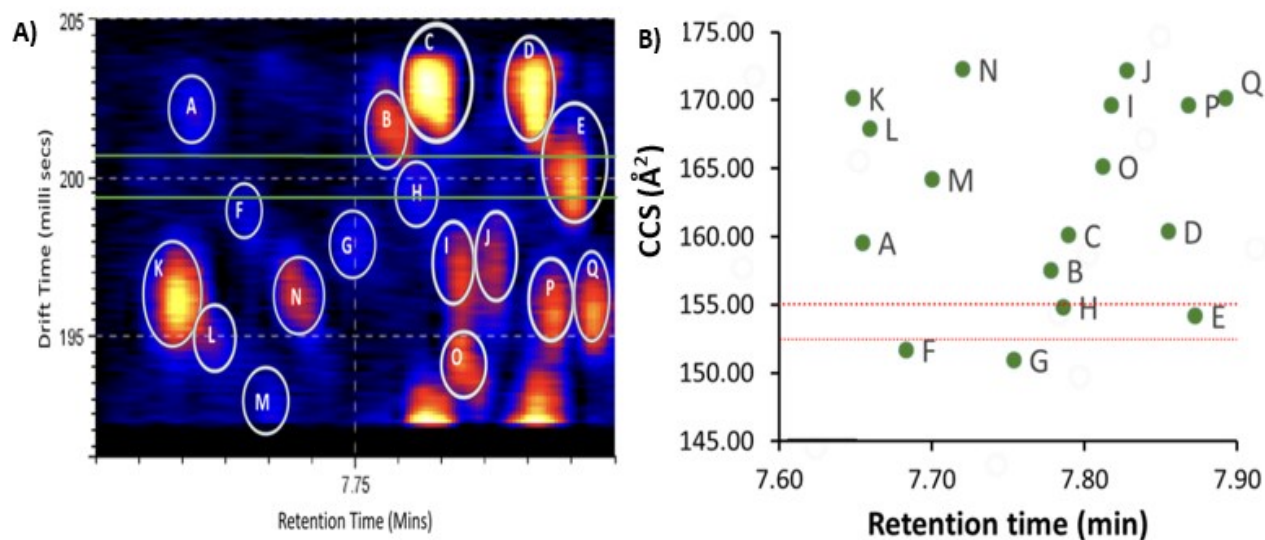
Figure 3.4. The plot of A) drift time (ms) and B) the CCS ($Å^2$) vs retention time (min)

3.5. Conclusion

The main objective of this study was to develop a method for analyzing data and differentiating toxic isomers. The results of this study have demonstrated the fast separation of isomers without the need for more sample preparation steps. However, all compounds are not able to resolve in one pass experiment, the cyclic ion mobility enabled the separation of isomers in multi-pass experiment. In addition, wrap-around of data points during multi-pass experiments was addressed by an unwrapping procedure. This example showed the unwrapping method is an effective procedure during utilizing complex matrices. Also, calculation of the CCS is possible by utilizing the periodic drift times. In summary, this study highlighted the utilization of cyclic ion mobility and multi-pass experiments for separation and differentiation between toxic and non-toxic isomers.

3.6. References

[1] Hites, R. A. Dioxins: An Overview and History. *Environmental Science & Technology* **2011**, *45* (1), 16-20.

[2] Sabarwal, A.; Kumar, K.; Singh, R. P. Hazardous effects of chemical pesticides on human health–Cancer and other associated disorders. *Environmental Toxicology and Pharmacology* **2018**, *63*, 103-114.

[3] Verma, R.; Vinoda, K. S.; Papireddy, M.; Gowda, A. N. S. Toxic Pollutants from Plastic Waste-A Review. *Procedia Environmental Sciences* **2016**, *35*, 701-708.

[4] Fernando, S.; Jobst, K. J.; Taguchi, V. Y.; Helm, P. A.; Reiner, E. J.; McCarry, B. E. Identification of the halogenated compounds resulting from the 1997 Plastimet Inc. fire in Hamilton, Ontario, using comprehensive two-dimensional gas chromatography and (ultra) high resolution mass spectrometry. *Environmental Science and Technology* **2014**, *48* (18), 10656-10663.

[5] van den Berg, M.; Denison, M. S.; Birnbaum, L. S.; Devito, M. J.; Fiedler, H.; Falandysz, J.; Rose, M.; Schrenk, D.; Safe, S.; Tohyama, C.; et al. Polybrominated dibenzo-p-dioxins, dibenzofurans, and biphenyls: inclusion in the toxicity equivalency factor concept for dioxin-like compounds. *The journal of Toxicological Sciences* **2013**, *133* (2), 197-208.

[6] Sun, J.-L.; Zeng, H.; Ni, H.-G. Halogenated polycyclic aromatic hydrocarbons in the environment. *Chemosphere* **2013**, *90* (6), 1751-1759.

[7] Behnisch, P. A.; Hosoe, K.; Sakai, S.-i. Combinatorial bio/chemical analysis of dioxin and dioxin-like compounds in waste recycling, feed/food, humans/wildlife and the environment. *Environment International* **2001**, *27* (6), 495-519.

[8] Van den Berg, M.; Birnbaum, L. S.; Denison, M.; De Vito, M.; Farland, W.; Feeley, M.; Fiedler, H.; Hakansson, H.; Hanberg, A.; Haws, L.; et al. The 2005 World Health Organization Reevaluation of Human and Mammalian Toxic Equivalency Factors for Dioxins and Dioxin-Like Compounds. *Toxicological Sciences* **2006**, *93* (2), 223-241.

[9] Tanabe, S.; Kannan, N.; Subramanian, A.; Watanabe, S.; Tatsukawa, R. Highly toxic coplanar PCBs: Occurrence, source, persistency and toxic implications to wildlife and humans. *Environmental Pollution* **1987**, *47* (2), 147-163.

[10] Yang, L.; Wu, J.; Zheng, M.; Cao, Z.; Li, C.; Shi, M.; Liu, G. Non-target screening of organic pollutants and target analysis of halogenated polycyclic aromatic hydrocarbons in the atmosphere around metallurgical plants by high-resolution GC/Q-TOF-MS. *Environmental Sciences Europe* **2020**, *32* (1), 96.

[11] Bianco, A.; Neefjes, I.; Alfaouri, D.; Vehkamäki, H.; Kurtén, T.; Ahonen, L.; Passananti, M.; Kangasluoma, J. Separation of isomers using a differential mobility analyser (DMA): Comparison of experimental vs modelled ion mobility. *Talanta* **2022**, *243*, 123339.

[12] Fernando, S.; Green, M. K.; Organtini, K.; Dorman, F.; Jones, R.; Reiner, E. J.; Jobst, K. J. Differentiation of (mixed) halogenated dibenzo-p-dioxins by negative ion atmospheric pressure chemical ionization. *Analytical Chemistry* **2016**, *88* (10), 5205-5211.

[13] Groessl, M.; Graf, S.; Knochenmuss, R. High resolution ion mobility-mass spectrometry for separation and identification of isomeric lipids. *Analyst* **2015**, *140* (20), 6904-6911.

[14] Yang, H.; Shi, L.; Zhuang, X.; Su, R.; Wan, D.; Song, F.; Li, J.; Liu, S. Identification of structurally closely related monosaccharide and disaccharide isomers by PMP labeling in conjunction with IM-MS/MS. *Scientific Reports* **2016**, *6* (1), 28079.

[15] Iacob, R. E.; Murphy, J. P., 3rd; Engen, J. R. Ion mobility adds an additional dimension to mass spectrometric analysis of solution-phase hydrogen/deuterium exchange. *Rapid Communication in Mass Spectromtry* **2008**, *22* (18), 2898-2904.

[16] Li, H.; Bendiak, B.; Siems, W. F.; Gang, D. R.; Hill, H. H., Jr. Ion mobility mass spectrometry analysis of isomeric disaccharide precursor, product and cluster ions. *Rapid Communication in Mass Spectromtry* **2013**, *27* (23), 2699-2709.

[17] May, J. C.; Morris, C. B.; McLean, J. A. Ion Mobility Collision Cross Section Compendium. *Analytical Chemistry* **2017**, *89* (2), 1032-1044.

[18] Fenn, L. S.; McLean, J. A. Structural resolution of carbohydrate positional and structural isomers based on gas-phase ion mobility-mass spectrometry. *Physical Chemistry Chemical Physics* **2011**, *13* (6), 2196-2205.

[19] Ujma, J.; Ropartz, D.; Giles, K.; Richardson, K.; Langridge, D.; Wildgoose, J.; Green, M.; Pringle, S. Cyclic Ion Mobility Mass Spectrometry Distinguishes Anomers and Open-Ring Forms of Pentasaccharides. *Journal of the American Society for Mass Spectrometry* **2019**, *30* (6), 1028-1037.

[20] Williamson, D. L.; Bergman, A. E.; Nagy, G. Investigating the Structure of α/β Carbohydrate Linkage Isomers as a Function of Group I Metal Adduction and Degree of Polymerization as Revealed by Cyclic Ion Mobility Separations. *Journal of the American Society for Mass Spectrometry* **2021**, *32* (10), 2573-2582.

[21] Giles, K.; Ujma, J.; Wildgoose, J.; Pringle, S.; Richardson, K.; Langridge, D.; Green, M. A Cyclic Ion Mobility-Mass Spectrometry System. *Analytical Chemistry* **2019**, *91* (13), 8564-8573.

[22] Steeves, K. L.; Bissram, M. J.; Kleywegt, S.; Stevens, D.; Dorman, F. L.; Simpson, A. J.; Simpson, M. J.; Cahill, L. S.; Jobst, K. J. Nontargeted screening reveals fluorotelomer ethoxylates in indoor dust and industrial wastewater. *Environment International* **2023**, *171*, 107634.

[23] Breen, J.; Hashemihedeshi, M.; Amiri, R.; Dorman, F. L.; Jobst, K. J. Unwrapping Wrap-around in Gas (or Liquid) Chromatographic Cyclic Ion Mobility–Mass Spectrometry. *Analytical Chemistry* **2022**, *94* (32), 11113-11117.

[24] Myers, A. L.; Mabury, S. A.; Reiner, E. J. Analysis of mixed halogenated dibenzo-p-dioxins and dibenzofurans (PXDD/PXDFs) in soil by gas chromatography tandem mass spectrometry (GC–MS/MS). *Chemosphere* **2012**, *87* (9), 1063-1069.

[25] Righetti, L.; Bergmann, A.; Galaverna, G.; Rolfsson, O.; Paglia, G.; Dall'Asta, C. Ion mobility-derived collision cross section database: Application to mycotoxin analysis. *Analytica Chimica Acta* **2018**, *1014*, 50-57.

[26] Mesleh, M. F.; Hunter, J. M.; Shvartsburg, A. A.; Schatz, G. C.; Jarrold, M. F. Structural Information from Ion Mobility Measurements: Effects of the Long-Range Potential. *The Journal of Physical Chemistry* **1996**, *100* (40), 16082-16086.

[27] Gabelica, V.; Shvartsburg, A. A.; Afonso, C.; Barran, P.; Benesch, J. L. P.; Bleiholder, C.; Bowers, M. T.; Bilbao, A.; Bush, M. F.; Campbell, J. L.; et al. Recommendations for reporting ion mobility Mass Spectrometry measurements. *Mass Spectromtry Reviews* **2019**, *38* (3), 291-320.

[28] Ruotolo, B. T.; Benesch, J. L.; Sandercock, A. M.; Hyung, S.-J.; Robinson, C. V. Ion mobility–mass spectrometry analysis of large protein complexes. *Nature Protocols* **2008**, *3* (7), 1139-1152.

Chapter 4

4.1. Conclusion

The presence of MNPs in different environments has raised concerns. Previous studies have shown the negative effects of exposure to MNPs [1, 2], their additives [3], and byproducts of plastic waste [4]. In this thesis, essential steps regarding these concerns were mentioned and a method for identifying and quantifying MNPs in indoor air was introduced.

For the first part of our research, two environments were selected for air sampling, laboratories and private residences, for the study of MNPs in indoor air. The results of this study demonstrated that the concentration of MNPs in the indoor air is higher than outdoor air by a factor of up to 1000 times [5]. The high concentration of MNPs measured in a living space and a workplace, underscores the need for more exploration of indoor air quality. The future investigation involves expanding the research to various indoor locations. The goal is to determine the differences in plastic concentrations depending on the types of furniture in these spaces and explore the effect of ventilation system on concentration of MNPs in indoor environments.

The presence of MNPs in indoor environments demonstrates a high risk of exposure. Also, it is worth considering that the smaller NPs could bioaccumulate rapidly and this leads to increased toxicity. Furthermore, smaller plastic particles can penetrate deeply into the respiratory system, including the human lungs. Not only can these NPs enter the bloodstream, but they can also accumulate in various organs, such as the placenta. The study by Aghaei et al. showed the exposure to PS-MNP can cause insufficient placental transfer, abnormal placental metabolism, and growth retardation in mice [6]. However, it is essential to mention that detecting and quantifying

NPs in complex matrices such as tissue is a challenge due to their size and matrix effect. Future studies will be developing methods for identifying and quantifying MNPs in various human and animal organs, including the placenta to measure NP concentrations to evaluate total human exposure to indoor air.

Moreover, the present has highlighted a correlation between the quantity of PUF and its additives, TDCPP. This correlation underscores the necessity for robust quantification methods. Notably, plastic particles carry toxic additives and transport persistent organic pollutants (POPs), which can potentially enter the human body. POPs can employ NPs as vectors for transfer in human body and bioaccumulate there. Despite this fact, the scientists need to do more investigation for sampling, identification and quantification of MNPs and POPs and the correlation between them in the environments that they originated.

Finally, cIM-MS offers an extra dimension of separation to the chromatographic methods such as GC. Samples with complex matrices, such as soil collected from location that fire happened there, contain thousands of possible HPAHs, which are not available as authentic standards. In the study of Plastimet samples, cIM-MS technique was utilized as a powerful tool to improve separation of TCA isomers through multi-pass experiment. The knowledge about CCS and findings from this experiment assist to detect the potential toxic TCA in the real sample with complex matrices. This achievement shows the ability to differentiate between potentially toxic and non-toxic variants of compounds that their authentic standard is not available. This emphasizes that the innovative method could be applied to real samples for identification approach.

In summary, the results of this thesis show high concentration of MNPs in indoor air and highlight the risks associated with exposure to plastic particles due to the volume of air that they are breathing daily. Therefore, exposure to MNPs in indoor environments can have serious risks

for human health and there is a need for more investigation in this area.

4.2. References

[1] Xu, J.-L.; Lin, X.; Wang, J. J.; Gowen, A. A. A review of potential human health impacts of micro- and nanoplastics exposure. *Science of the Total Environment* **2022**, *851*, 158111.

[2] Rodrigues, A. C. B.; de Jesus, G. P.; Waked, D.; Gomes, G. L.; Silva, T. M.; Yariwake, V. Y.; da Silva, M. P.; Magaldi, A. J.; Veras, M. M. Scientific Evidence about the Risks of Micro and Nanoplastics (MNPLs) to Human Health and Their Exposure Routes through the Environment. *Toxics* **2022**, *10* (6), 308.

[3] Hahladakis, J. N.; Velis, C. A.; Weber, R.; Iacovidou, E.; Purnell, P. An overview of chemical additives present in plastics: Migration, release, fate and environmental impact during their use, disposal and recycling. *Journal of Hazardous Materials* **2018**, *344*, 179-199.

[4] Islam, M. R.; Welker, J.; Salam, A.; Stone, E. A. Plastic Burning Impacts on Atmospheric Fine Particulate Matter at Urban and Rural Sites in the USA and Bangladesh. *ACS Environmental Au* **2022**, *2* (5), 409-417.

[5] Costa-Gómez, I.; Suarez-Suarez, M.; Moreno, J. M.; Moreno-Grau, S.; Negral, L.; Arroyo-Manzanares, N.; López-García, I.; Peñalver, R. A novel application of thermogravimetry-mass spectrometry for polystyrene quantification in the PM10 and PM2.5 fractions of airborne microplastics. *Science of the Total Environment* **2023**, *856*, 159041.

[6] Aghaei, Z.; Sled, J. G.; Kingdom, J. C.; Baschat, A. A.; Helm, P. A.; Jobst, K. J.; Cahill, L. S. Maternal Exposure to Polystyrene Micro- and Nanoplastics Causes Fetal Growth Restriction in Mice. *Environmental Science & Technology Letters* **2022**, *9* (5), 426-430.